the corresponding RI7 regions could also improve the functions of other ORs, such as the transportation capability and the ligand responsiveness, in the yeast cells.

The Effects of Substituting the Endogenous Gα Subunit, Gpa1, With the Olfactory Gα Subunit, G_{olf}

To improve the coupling between ORs and their corresponding G-proteins, we tested the effects of co-expression of the OR-specific Gα subunit, G_{olf}, with $cI7_{N58}$OR226 in a *gpa1*Δ yeast strain (FL150-$cI7_{N58}$OR226-Golf, abbreviated as cOR226-Golf; Table I). For comparison, we additionally prepared two yeast transformants that either expressed the chimeric OR with the endogenous Gpa1 protein (FL50-$cI7_{N58}$OR226 expressing endogenous Gpa1, abbreviated as cOR226-Gpa1; Table I) or G_{olf} alone without the chimeric OR (FL150-ΔOR-Golf, abbreviated as ΔOR-Golf; Table I). The *gpa1*Δ strain containing G_{olf} (cOR226-Golf) exhibited similar expression levels of the chimeric OR to the Gpa1-expressing strain (cOR226-Gpa1). This result indicated that the substitution of the G-protein α-subunit had no negative effects on the expression of the OR (Fig. 5).

Consequently, the responsiveness of the chimeric OR toward DNT drastically was increased by introducing G_{olf} in place of Gpa1 (Fig. 6). The yeast strain with the chimeric OR (cOR226-Golf) exhibited higher bioluminescence intensities compared to the strain without the OR (ΔOR-Golf) even in the absence of DNT, which was likely due to a weak signal

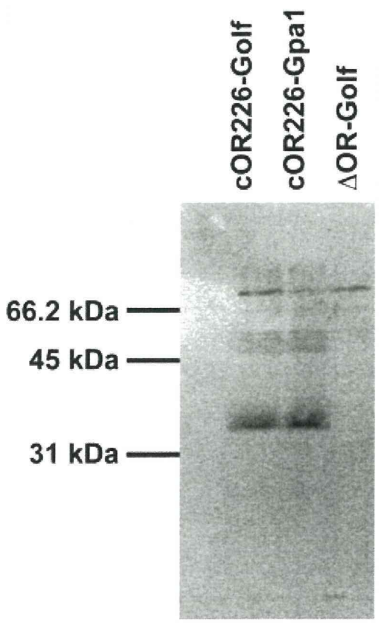

Figure 5. The expression of the $cI7_{N58}$OR226 chimeric receptor in G_{olf}-expressing yeast. FL150-$cI7_{N58}$OR226-Golf (cOR226-Golf), FL50-$cI7_{N58}$OR226 (cOR226-Gpa1), and FL150-ΔOR-Golf (ΔOR-Golf) yeast transformants were used to compare the expression levels of the $cI7_{N58}$OR226 chimeric receptor. An immunoblot analysis of the $cI7_{N58}$OR226 chimeric receptors was performed on yeast whole-cell extracts with a HRP-conjugated anti-c-myc antibody.

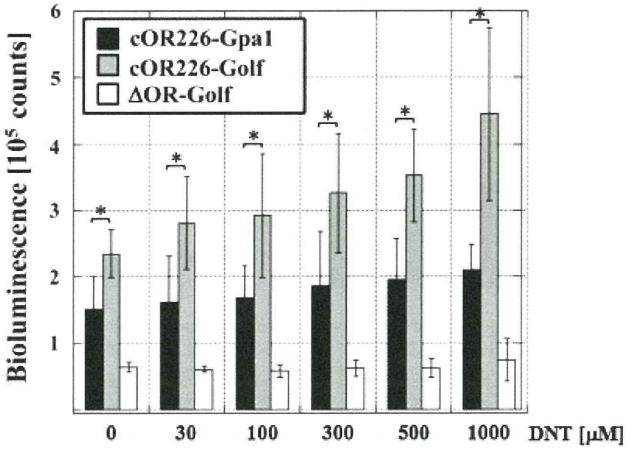

Figure 6. DNT sensing using the *luc* reporter gene assay in yeast cells co-expressing the $cI7_{N58}$OR226 chimeric receptor with G_{olf}. FL150-$cI7_{N58}$OR226-Golf (cOR226-Golf), FL50-$cI7_{N58}$OR226 (cOR226-Gpa1), and FL150-ΔOR-Golf (ΔOR-Golf) yeast transformants were tested for their ability to sense the odorant DNT. Bioluminescence was measured in the yeast strains stimulated by addition of DNT in the middle of cultivation in SGR media. The data shown represent the mean ± SEM of three separate experiments. Statistical significance was assessed by the *t*-test (*$P < 0.05$). The luminescence values for the negative control (cOR226-Gpa1) can be found in Figure 4.

generated by the coupling of the OR with G_{olf} in the absence of ligand. However, the expression of G_{olf} clearly offered advantages for odor sensing in the OR-expressing yeast. These advantages were evident by an increase in the dose-dependent responsiveness toward the DNT ligand with G_{olf} expression. Although it has been previously suggested that the expression of G_{olf} improved the signaling in the yeast with the whole RI7 receptor, our results also showed that the substitution of Gpa1 with G_{olf} enabled a highly effective coupling between G_{olf} and the long chimeric RI7/mOR226 ($cI7_{N58}$OR226) and permitted the use of a highly sensitive reporter gene assay. Because a dose-dependent responsiveness for DNT could not be observed using the fluorescent *GFP* reporter gene, our odor-sensing system with the *luc* reporter was clearly more sensitive (Supplementary Fig. S1). Thus, our arguments in this study were successfully demonstrated, although additional endeavors to confer a more vivid dose-dependency would be needed. Compared to other GPCRs, relatively scarce responses might be due to the binding flexibility of the odor ligand to the ORs (Malnic et al., 1999). To address this issue, fundamental innovations such as a strategy to amplify the G-protein signaling triggered by the agonist stimulation in yeast (Fukuda et al., 2011) may be helpful. This technique driven only by introducing an artificial signal activator could serve as the interface for elevating our approach to a more reliable sensing tool. As odorants are mainly hydrophobic, it is also important to increase their solubility in aqueous solution to detect ORs. Many animals secrete odorant binding proteins in nasal mucus. The solubility of odorants is enhanced via odorant binding proteins that exist in the extracellular fluid

surrounding the odorant receptors (Vogt et al., 1991). Similar method or other odorant concentrating system should be developed for the biomimetic sensors.

Conclusion

Here, we demonstrated that the replacement of the mOR226 N-terminal region, including the TM1 and ICL1 domains, by the corresponding regions of the RI7 receptor enhances the activity of the chimeric OR for odor sensing in yeast. This chimeric RI7/mOR226 receptor enhanced the expression of the OR on the yeast cell surface membrane and the signal transduction stimulated from the external ligand though the endogenous yeast G-protein signaling pathway. Although the generality of our design should be proven in the future, the *luc* reporter gene system we implemented was highly sensitive compared to the *GFP* reporter gene for odor sensing. Furthermore, the strategy of substituting the endogenous yeast Gα subunit with the olfactory specific G_{olf} appeared to improve the coupling efficiency between the OR and the G-protein, which indicated this strategy may be applicable for establishing an odor sensor system with OR-expressing yeast. Our efforts in this study provide beneficial information for the development of a more complete and advanced yeast-based biomimetic odor-sensing system.

We are grateful to Prof. K. Tohara from Tokyo University for providing the Golf gene construct. The work reported here is partly supported by Secom Science and Technology Foundation.

References

Bargmann CI. 2006. Comparative chemosensation from receptors to ecology. Nature 444(7117):295–301.

Brachmann CB, Davies A, Cost GJ, Caputo E, Li J, Hieter P, Boeke JD. 1998. Designer deletion strains derived from *Saccharomyces cerevisiae* S288C: A useful set of strains and plasmids for PCR-mediated gene disruption and other applications. Yeast 14(2):115–132.

Buck L, Axel R. 1991. A novel multigene family may encode odorant receptors: A molecular basis for odor recognition. Cell 65(1):175–187.

Chess A, Simon I, Cedar H, Axel R. 1994. Allelic inactivation regulates olfactory receptor gene expression. Cell 78(5):823–834.

Fukuda N, Yomogida K, Okabe M, Touhara K. 2004. Functional characterization of a mouse testicular olfactory receptor and its role in chemosensing and in regulation of sperm motility. J Cell Sci 117(Pt 24):5835–5845.

Fukuda T, Shiraga S, Kato M, Suye S, Ueda M. 2006. Construction of a cultivation system of a yeast single cell in a cell chip microchamber. Biotechnol Prog 22(4):944–948.

Fukuda N, Ishii J, Kaishima M, Kondo A. 2011. Amplification of agonist stimulation of human G-protein-coupled receptor signaling in yeast. Anal Biochem 417(2):182–187.

Hatt H, Gisselmann G, Wetzel CH. 1999. Cloning, functional expression and characterization of a human olfactory receptor. Cell Mol Biol 45(3):285–291.

Iguchi Y, Ishii J, Nakayama H, Ishikura A, Izawa K, Tanaka T, Ogino C, Kondo A. 2010. Control of signalling properties of human somatostatin receptor subtype-5 by additional signal sequences on its amino-terminus in yeast. J Biochem 147(6):875–884.

Ishii J, Tanaka T, Matsumura S, Tatematsu K, Kuroda S, Ogino C, Fukuda H, Kondo A. 2008. Yeast-based fluorescence reporter assay of G protein-coupled receptor signalling for flow cytometric screening: FAR1-disruption recovers loss of episomal plasmid caused by signalling in yeast. J Biochem 143(5):667–674.

Ishii J, Izawa K, Matsumura S, Wakamura K, Tanino T, Tanaka T, Ogino C, Fukuda H, Kondo A. 2009. A simple and immediate method for simultaneously evaluating expression level and plasmid maintenance in yeast. J Biochem 145(6):701–708.

Ishii J, Fukuda N, Tanaka T, Ogino C, Kondo A. 2010. Protein–protein interactions and selection: Yeast-based approaches that exploit guanine nucleotide-binding protein signaling. FEBS J 277(9):1982–1995.

Katada S, Nakagawa T, Kataoka H, Touhara K. 2003. Odorant response assays for a heterologously expressed olfactory receptor. Biochem Biophys Res Commun 305(4):964–969.

Krautwurst D, Yau KW, Reed RR. 1998. Identification of ligands for olfactory receptors by functional expression of a receptor library. Cell 95(7):917–926.

Ladds G, Goddard A, Davey J. 2005. Functional analysis of heterologous GPCR signalling pathways in yeast. Trends Biotechnol 23(7):367–373.

Malnic B, Hirono J, Sato T, Buck LB. 1999. Combinatorial receptor codes for odors. Cell 96(5):713–723.

Marrakchi M, Vidic J, Jaffrezic-Renault N, Martelet C, Pajot-Augy E. 2007. A new concept of olfactory biosensor based on interdigitated microelectrodes and immobilized yeasts expressing the human receptor OR17-40. Eur Biophys J 36(8):1015–1018.

Minic J, Persuy MA, Godel E, Aioun J, Connerton I, Salesse R, Pajot-Augy E. 2005a. Functional expression of olfactory receptors in yeast and development of a bioassay for odorant screening. FEBS J 272(2):524–537.

Minic J, Sautel M, Salesse R, Pajot-Augy E. 2005b. Yeast system as a screening tool for pharmacological assessment of g protein coupled receptors. Curr Med Chem 12(8):961–969.

Nei M, Niimura Y, Nozawa M. 2008. The evolution of animal chemosensory receptor gene repertoires: Roles of chance and necessity. Nat Rev Genet 9(12):951–963.

Niimura Y, Nei M. 2005. Evolutionary dynamics of olfactory receptor genes in fishes and tetrapods. Proc Natl Acad Sci USA 102(17):6039–6044.

O'Malley MA, Mancini JD, Young CL, McCusker EC, Raden D, Robinson AS. 2009. Progress toward heterologous expression of active G-protein-coupled receptors in *Saccharomyces cerevisiae*: Linking cellular stress response with translocation and trafficking. Protein Sci 18(11):2356–2370.

Pausch MH, Lai M, Tseng E, Paulsen J, Bates B, Kwak S. 2004. Functional expression of human and mouse P2Y12 receptors in *Saccharomyces cerevisiae*. Biochem Biophys Res Commun 324(1):171–177.

Price LA, Kajkowski EM, Hadcock JR, Ozenberger BA, Pausch MH. 1995. Functional coupling of a mammalian somatostatin receptor to the yeast pheromone response pathway. Mol Cell Biol 15(11):6188–6195.

Radhika V, Proikas-Cezanne T, Jayaraman M, Onesime D, Ha JH, Dhanasekaran DN. 2007. Chemical sensing of DNT by engineered olfactory yeast strain. Nat Chem Biol 3(6):325–330.

Schiestl RH, Dominska M, Petes TD. 1993. Transformation of *Saccharomyces cerevisiae* with non-homologous DNA: Illegitimate integration of transforming DNA into yeast chromosomes and in vivo ligation of transforming DNA to mitochondrial DNA sequences. Mol Cell Biol 13(5):2697–2705.

Saito H, Kubota M, Roberts RW, Chi Q, Matsunami H. 2004. RTP family members induce functional expression of mammalian odorant receptors. Cell 119(5):679–691.

Serizawa S, Miyamichi K, Nakatani H, Suzuki M, Saito M, Yoshihara Y, Sakano H. 2003. Negative feedback regulation ensures the one receptor-one olfactory neuron rule in mouse. Science 302(5653):2088–2094.

Togawa S, Ishii J, Ishikura A, Tanaka T, Ogino C, Kondo A. 2010. Importance of asparagine residues at positions 13 and 26 on the amino-terminal domain of human somatostatin receptor subtype-5 in signalling. J Biochem 147(6):867–873.

Vogt RG, Prestwich GD, Lerner MR. 1991. Odorant-binding-protein subfamilies associate with distinct classes of olfactory receptor neurons in insects. J Neurobiol 22(1):74–84.

Zhang X, Firestein S. 2002. The olfactory receptor gene superfamily of the mouse. Nat Neurosci 5(2):124–133.

Biotechnol. J. 2011, 6 DOI 10.1002/biot.201100213 www.biotechnology-journal.com

Technical Report

Site-specific protein labeling with amine-containing molecules using *Lactobacillus plantarum* sortase

Takuya Matsumoto[1], Ryosuke Takase[1], Tsutomu Tanaka[2], Hideki Fukuda[2] and Akihiko Kondo[1]

[1]Department of Chemical Science and Engineering, Graduate School of Engineering, Kobe University, Nada, Kobe, Japan
[2]Organization of Advanced Science and Technology, Kobe University, Nada, Kobe, Japan

Modification of proteins with small molecules is a widely used and powerful tool in biological research. Enzymatic approaches are particularly promising because substrate specificity allows for site-specific modification. Sortase A, a transpeptidase from *Staphylococcus aureus*, cleaves between the T and G residues in the sequence LPXTG, and subsequently links the carboxyl group of the T residue to an amino group of N-terminal glycine oligomers by a native peptide bond. Although Gram-positive bacteria have several kinds of sortases, there are few reports concerning their expression and substrate specificity. Here, we demonstrate site-specific protein modification with primary amine-containing molecules catalyzed by *Lactobacillus plantarum* sortase. Enhanced green fluorescent protein (EGFP) was employed as a model protein, and an amine-containing biotin molecule was site-specifically conjugated with LPQTSEQ-tagged EGFP. We developed a novel *Lactobacillus plantarum* sortase that has different substrate specificity compared to *Staphylococcus aureus* sortase. Amine-directed protein modification was achieved using the *Lactobacillus plantarum* sortase "LPQTSEQ" sequence original recognition tag. Our results demonstrate a promising method for expanding the capabilities of site-specific protein-small molecule modification.

Received 6 April 2011
Revised 19 August 2011
Accepted 13 September 2011

Keywords: Protein engineering · Protein modification · Sortase

1 Introduction

Modifying proteins with small molecules is a widely used and powerful tool for biological research. For instance, modifying proteins with fluorescein or functional aptamers is used for labeling and/or imaging [1–4], and modifying proteins with magnetic nanoparticles is useful for protein purification or separation [5, 6]. Protein-small molecule conjugates can be generated by either covalent or non-covalent binding. Chemical modification or biotin–streptavidin interaction is often used, although this strategy is not always "site-specific," and therefore the products generated by such "random modification" are often heterogeneous or loss of functions [1–6].

Site-specific protein modification is a much more attractive strategy because it enables protein manipulation without significant loss of function. The property of substrate specificity makes enzymatic approaches ideally suited for site-specific protein modification. Transglutaminase (TGase) is a protein-coupling enzyme that catalyzes an acyl transfer reaction between the γ-carboxyamine group of glutamine (Q) residues and the ε-amino group of lysine (K) residues or various other primary amines. Several TGase enzymes have been used for modifying proteins with primary amine-containing molecules such as fluorescence probes or PEG [7–9]. In this approach, a short substrate sequence for transglutaminase is genetically introduced at the N- or C-terminus of the target protein. The expressed protein is then modified with a small primary amine-containing molecule. The advantages of this enzymatic protein modification

Correspondence: Dr. Tsutomu Tanaka, Organization of Advanced Science and Technology, Kobe University, 1-1 Rokkodaicho, Nada, Kobe 657-8501, Japan
E-mail: tanaka@kitty.kobe-u.ac.jp

Abbreviations: EGFP, enhanced green fluorescent protein; **SrtA**, sortase A; **TGase**, transglutaminase

strategy are that it is highly selective and is mild compared to conventional methods. However, the variety of peptidyl tags useful as substrates for TGase is currently limited because the substrate specificity of this class of enzymes has not been clearly established. Another limitation is that the variation of TGase and its recombinant expression system has not been sufficiently developed [10].

Use of the transpeptidase enzyme sortase for protein modification has increased recently [10–20]. Sortase A (SrtA), isolated from *Staphylococcus aureus*, is one of the most well-studied sortases. Sortase is present on the cell surface of Gram-positive bacteria and catalyzes the covalent linkage of surface proteins to cell wall peptidoglycan, a process that is critical for bacterial infection of the host [10–12]. SrtA recognizes the sequence LPXTG, cleaves between the T and G residues, and subsequently links the carboxyl group of the T residue to an amino group of N-terminal glycine oligomers through a native peptide bond. Recombinant soluble SrtA has been used for protein-protein, peptide, and small molecule ligation in vitro because of its greater substrate specificity [13–16]. Several interesting applications using sortase, such as dual labeling and protein circularization, have been reported [17–20]. Although Gram-positive bacteria possess several sortases of varying substrate specificity, there are few reports regarding their expression and substrate specificity [18, 19].

In this study, we demonstrate site-specific protein modification with primary amine-containing molecules catalyzed by a sortase from *Lactobacillus plantarum*. First, several putative sortases from *Lactobacillus plantarum*, *Lactococcus lactis*, and *Corynebacterium glutamicum* were cloned and expressed using *E. coli* as the host. Enhanced green fluorescent protein (EGFP) containing a LPXTG motif sequence at its C-terminus was employed as a model protein, while an amine-containing biotin molecule (amine-PEO_2-biotin) was employed as a model substrate. In the case of *L. plantarum* sortase, amine-PEO_2-biotin was site-specifically conjugated with LPQTSEQ-tagged EGFP and had a different substrate specificity than *S. aureus* sortase. In addition, we demonstrate site-specific protein immobilization on amine-modified microbeads.

2 Materials and methods

2.1 Chemicals and materials

TALON metal affinity resin, (+)-biotinyl-3,6-dioxaoctanediamine (Amine-PEO_2-biotin) and the BCA protein assay kit were purchased from TAKARA-BIO, inc Shiga, Japan Amine-coated microbeads (micromere-NH_2) was from micromod Partikeltechnologie GmbH, Germany. Streptavidin alkaline phosphatase conjugate, BCIP and NBT (detection for reagent of western blotting) were purchased from Promega Corporation, Madison, WI, USA. All other chemicals were purchased from Nacalai Tesque, Kyoto, Japan. SDS-PAGE analysis was performed using PowerPac Basic (Bio-Rad Laboratories, Hercules, CA, USA) and western blotting was performed using from AE-6677 HorizBLOT (ATTO Corporation, Tokyo, Japan).

2.2 Cloning, expression, and purification of sortases

The sortase gene from *Lactobacillus plantarum* NCIMB 8826 (Accession: NP_784294) was amplified using the following primers: 5′-GGTACCGGATCCAACTTCTCAAAGGTCAAGTCACTTGAC-3′ and 5′-GCGAGCTCGAATTCTTAATATTTGTTATTAAAATGACTTGTAAAGGCC-3′. The sortase genes from *Lactococcus lactis* IL1403 (yhhA: NP_266915 and ylcC: NP_267269) and *Corynebacterium glutamicum* (NP_602126) were amplified from the *L. lactis* IL1403 or *C. glutamicum* ATCC 13032 genomes using the following primers: 5′-GCGGTACCGGATCCGGAAGTGCTAAAGTAAAGGAATTGCTTAGTC-3′ and 5′-GCGAGCTCGAATTCCTACTTTTTGTCAATTATCCCTCCCCCTTTC-3′ (yhhA), 5′-GCGGTACCGGATCCTTTAAATCTTGCTATACGCAAGATTTTTTTGTAAAAC-3′ and 5′-GCGAGCTCGAATTCCTAGAAATTTTTAATTTGATTATATTTGGTTTCAAATGC-3′ (ylcC), 5′-GCGGTACCGGATCCCAAAAGCTTGATGAAGACTGGAATGAAGC-3′ and 5′-GCGAGCTCGAATTCTTAGTTTTTCCTCCAAAGCTGCAGGGCGTTCGCC-3′ (NP_602126).

The amplified fragments were digested with *Kpn*I/*Sac*I and ligated into pBAD-Gly5-EGFP [21]. The resultant plasmid was transformed into Top10 (Invitrogen) and expressed by induction with 0.1% L-arabinose at 25°C overnight. The cell pellets were resuspended in 50 mM phosphate, 150 mM NaCl, pH 8.0 and lysed by sonication. The expressed proteins in soluble fractions were purified using TALON metal affinity resins according to the manufacturer's protocol. Purified sortases were dialyzed against 20 mM Tris/150 mM NaCl, pH 8. The protein concentration was determined using the BCA protein assay kit.

2.3 Specific-tagged EGFP preparation

Site-directed mutagenesis analysis was carried out using a QuikChange site-directed mutagenesis kit

(Stratagene) with pBAD-Gly5-EGFP as the template. The primer sequences were as follows: 5′-CGGCATGGACGAGCTGTACAAGGGCTCTCTG GCGGCCACTGGTTGGATGGGTTCC TAGGAGC TCAAGGGCGAGCTTGAAGG-3′ (EGFP-LA), 5′-CGGCATGGACGAGCTGTACAAGGGCTCTCTG CCTAAGACTGGCGACGACGGTTCC TAGGAGC TCAAGGGCGAGCTTGAAGG-3′ (EGFP-LK), 5′-CGGCATGGACGAGCTGTACAAGGGCTCTCTG CCTCAGACTTCCGAGCAGGGTTCC TAGGAGCT CAAGGGCGAGCTTGAAGG-3′ (EGFP-LQ), 5′-GAGCTCCTAGGAACCCTGCTCCGCAGTCTG AGGCAGAGAGCCCTTGTAC-3′ (EGFP-QcH1), 5′-GAGCTCCTAGGAACCCTGCTCAGTAGTCTG AGGCAGAGAGCCCTTGTAC-3′ (EGFP-QcH2), 5′-GAGCTCCTAGGAACCCTGCTCCACAGTCTG AGGCAGAGAGCCCTTGTAC-3′ (EGFP-QcH3), 5′-GAGCTCCTAGGAACCCTGCTCAGTCTGAGG CAGAGAGCCCTTGTAC-3′ (EGFP-QcH4), 5′-GA GCTCCTAGGAACCCTGCTCCTGAGGCAGAG AGCCCTTGTAC-3′ (EGFP-QcH5), 5′-GAGCTCCT AGGAACCCTGCTCACCAGTGGCCCACAGAG AGCCCTTGTAC-3′ (EGFP-QcH6), 5′-GAGCTCC TAGGAACCCTGCTCGGAAGTGGCCCACAGAG AGCCCTTGTAC-3′ (EGFP-QcH7), 5′-GAGCTCCT AGGAACCCTGCTCACCAGTGGCGTGCAGAGA GCCCTTGTAC-3′ (EGFP-QcH8), 5′-GAGCTCCTA GGAACCCTGCTCGGAAGTGGCGTGCAGAGAG CCCTTGTAC-3′ (EGFP-QcH9), 5′-GAGCTCCTAG GAACCCTGCTCCTTAGTCTGAGGCAGAGAGCC CTTGTAC-3′ (EGFP-QcH10), 5′-GAGCTCCTAGG AACCCTGCTCCCTAGTCTGAGGCAGAGAGCCC TTGTAC-3′ (EGFP-QcH11), 5′-GAGCTCCTAGGA ACCCTGCTCGAAAGTCTGAGGCAGAGAGCCCT TGTAC-3′ (EGFP-QcH12), 5′-GAGCTCCTAGGAA CCCTGCTCCTTAGTCTGAGGCAGAGAGCCCTT GTAC-3′ (EGFP-QcH13), 5′-GAGCTCCTAGGAAC CACCAGTCTGAGGCAGAGAGCCCTTGTAC-3′ (EGFP-QcH14), 5′-GAGCTCCTAGGAACCCTGCT CGGAGGCCTGAGGCAGAGAGCCCTTGTAC-3′ (EGFP-QcH15), 5′-GAGCTCCTAGGAACCCTGCT CACCGGCCTGAGGCAGAGAGCCCTTGTAC-3′ (EGFP-QcH16), 5′-GAGCTCCTAGGAACCCTGCT CGGACCTCTGAGGCAGAGAGCCCTTGTAC-3′ (EGFP-QcH17), 5′-GAGCTCCTAGGAACCCTGCT CACCCCTCTGAGGCAGAGAGCCCTTGTAC-3′ (EGFP-QcH18), 5′-CTAGGAACCCATCCAACCAG TCTCCGCCAGAGAGCCCTTGTACAGCTCG-3′ (EGFP-QcH19), and their complementary strands. The amino acid sequences of the C-terminal additional peptides are shown in Table 1.

2.4 Protein modification with amine-PEO_2-biotin using sortase

(+)-Biotinyl-3,6-dioxaoctanediamine (50 μM) and tagged-EGFP (5 μM) were dissolved in 20 mM sodium phosphate buffer (pH 8) and the enzymatic modification reaction was initiated by addition of sortase (5 μM). After incubation for 24 h at 37°C, the

Table 1. Modification of tagged EGFPs with amine-PEO2-biotin

Lane number	Tag name	Tag sequence	SrtLp modification	SrtA modification	Potential enzyme
1	QcH1	LPQTAEQ	Conjugated	Not conjugated	Variant
2	QcH2	LPQTTEQ	Not conjugated	Not conjugated	Variant
3	QcH3	LPQTVEQ	Not conjugated	Not conjugated	Variant
4	QcH4	LPQTEQ	Not conjugated	Not conjugated	Variant
5	QcH5	LPQEQ	Not conjugated	Not conjugated	Variant
6	QcH6	LWATGEQ	Not conjugated	Not conjugated	Variant
7	QcH7	LWATSEQ	Not conjugated	Not conjugated	Variant
8	QcH8	LHATGEQ	Not conjugated	Not conjugated	Variant
9	QcH9	LHATSEQ	Not conjugated	Not conjugated	Variant
10	QcH10	LPQTKEQ	Conjugated	Not conjugated	Variant
11	QcH11	LPQTREQ	Conjugated	Not conjugated	Variant
12	QcH12	LPQTFEQ	Conjugated	Not conjugated	Variant
13	QcH13	LPQTS	Conjugated	Not conjugated	Variant
14	QcH14	LPQTG	Conjugated	Conjugated	Variant
15	QcH15	LPQASEQ	Conjugated	Not conjugated	Variant
16	QcH16	LPQAGEQ	Conjugated	Conjugated	Variant
17	QcH17	LPQRSEQ	Not conjugated	Not conjugated	Variant
18	QcH18	LPQRGEQ	Not conjugated	Not conjugated	Variant
19	QcH19	LAETG	Conjugated	Conjugated	Variant
20	LA	LAATGWM	Conjugated	Conjugated	SrtCg
21	LK	LPKTGDD	Conjugated	Conjugated	SrtLl
22	LQ	LPQTSEQ	Conjugated	Not conjugated	SrtLp

reaction was terminated by addition of SDS-PAGE sample buffer (50 mM Tris–HCl, 2% SDS, 6% 2-mercaptoetahnol) followed by boiling. The samples were then subjected to SDS-PAGE and analyzed by western blotting with streptavidin-alkaline phosphatase and BCIP/NBT according to manufactures' procedure.

2.5 Protein modification with microbeads using SrtLp

Amine-coated microbeads (micromere-NH_2: 50 μg, 2 μm) and tagged-EGFP (5 μM) were dissolved in 20 mM sodium phosphate buffer (pH 8). The enzymatic modification reaction was initiated by addition of sortase (50 μM). Total reaction volume is 100 μL. After incubation for 24 h at 37°C, the beads were washed three times with PBS, dissolved PBS (20 μL), and directly observed using fluorescence microscopy.

3 Results and discussion

3.1 Preparation of novel sortases

Many Gram-positive bacteria produce sortases. We cloned and expressed sortase from *L. plantarum* (SrtLp), *L. lactis* (SrtLl), and *C. glutamicum* (SrtCg) using *E. coli* as a host. The sortase from *L. plantarum* is 234 a.a. and from *C. glutamicum* is 274 a.a., while the sortases from *L. lactis* (SrtLl-yhhA) (SrtLl-ylcC) are 432 and 287 a.a., respectively. The number of amino acid and the amino acid sequence was referred from sortase database (http://nih-server.mbi.ucla.edu/Sortase/) and their DNA sequences were confirmed. Each sortase has TLXTC motif, which is the active-site of sortase superfamily [11]. Generally, sortase is expressed on the cell surface and is retained there by cell wall anchoring motifs. With the exception of ylcC, all sortases have hydrophobic motifs at the N-terminus. When *E. coli* was used as a host, hydrophobic motifs causes sortase expression hard [22, 23], we trimmed 60 residues from the N-terminal region of each sortase. Figure 1A illustrates the results of SDS-PAGE analysis of the expressed sortases after His-tag purification. All sortases were successfully expressed as thioredoxin-fusion proteins in the soluble fraction. The size SrtLl-yhhA seems to be lower than expected, which might be non-specific digestion in *E. coli*. We were unable to express sortases from various other microorganisms, such as *Bacillus sp.*, *Clostridium sp.*, and *Streptomyces sp.* as soluble thioredoxin-fusion proteins in *E. coli* (data not shown).

3.2 Sortase reaction with LPXTG-tagged EGFP and Gly5-EGFP

The consensus sequence of sortase substrate proteins is LPXTG; hence, we screened for the LPXTG sequence in the original microorganisms *L. plantarum*, *L. lactis*, and *C. glutamicum*. In the *L. plantarum*, there are potential sortase substrate proteins containing the motifs LPQTSE and LPQTGE, also LPSTG, LPKTG, LPFTG and LPETG motifs in the *L. lactis*, LAATGWM motif in the *C. glutamicum*, respectivelly. All proteins are expected to be cell surface protein precursors and each motif is located in the C-terminal region.

Using EGFP as a model protein, we prepared EGFP carrying various LPXTG motifs at its C-terminus. The tag sequences are summarized in Table 1. SrtA can conjugate the LPXTG sequence with an N-terminal pentaglycine sequence; therefore, we first tested the reaction between tagged EGFP and Gly5-EGFP. Although SrtA was able to conjugate EGFP-LPXTG and Gly5-EGFP, none of the other sortases (SrtLl-yhhA, SrtLl-ylcC, SrtLp, or SrtCg) were able to conjugate EGFP-LPXXX (LPXTG or other potential substrate motif of each sortase) and Gly5-EGFP (data not shown).

3.3 Sortase reaction with tagged EGFP and amine-PEO_2-biotin

S. aureus SrtA was recently shown to conjugate the sequence LPXTG and primary amine-containing molecules [13, 16]. To further define the substrate specificity of sortases, we examined the ability of sortase to catalyze conjugation of EGFP and the amine-containing small molecule (+)-biotinyl-3,6-dioxaoctanediamine (amine-PEO_2-biotin). Amine-PEO_2-biotin is an ideal model substrate because the biotin moiety is easily detected. The sortase reaction between tagged EGFP and amine-PEO_2-biotin was carried out at 37°C. Figure 1B–D show western blotting analysis using streptavidin-AP after the SrtA or SrtLp reaction. Figure 1B shows western blot analysis of the sortase-mediated reaction between EGFP-LA (potential substrate motif of SrtCg) and amine-PEO_2-biotin, and demonstrates that both SrtA and SrtLp were able to conjugate tagged EGFP and amine-PEO_2-biotin. Similarly, EGFP-LK (potential substrate motif of SrtLl-yhhA and SrtLl-ylcC) and amione-PEO_2-biotin were successfully conjugated by SrtA or SrtLp (Fig. 1C). Other sortases (SrtLl-yhhA, SrtLl-ylcC, and SrtCg) were unable to conjugate tagged EGFP (LPXTG or other potential substrate motif of each sortase) and amine-PEO_2-biotin (data not shown), because SrtLl yhhA, ylcC and SrtCg are predicted

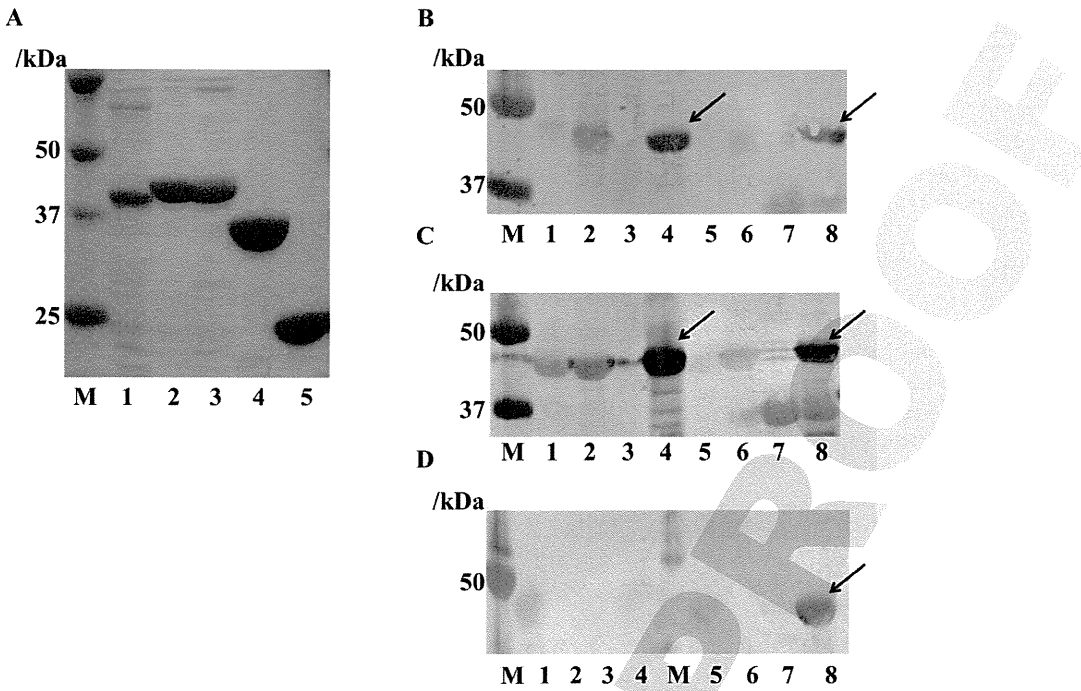

Figure 1. All sortases were expressed in *E. coli* and soluble fractions were purified by TALON metal affinity resin, then purified samples were analyzed SDS-PAGE. The sortase reaction product of tagged-EGFP and amine-PEO_2-biotin was analyzed by western blotting using streptavidin-HRP. (**A**) SDS-PAGE analysis of thioredoxin-sortase fusion proteins after His-tag purification. (Lane 1: SrtLl-yhhA; lane 2: SrtLl-ylcC; lane 3: SrtCg; lane 4: SrtLp; lane 5: SrtA; M: molecular weight markers). (**B**) Western blot analysis of the products of the site-specific reaction between EGFP-LA and amine-PEO_2-biotin after sortase treatment (The arrows show confirmed protein modification. Lane 1: EGFP-LA; lane 2: EGFP-LA and amine-PEO_2-biotin; lane 3: amine-PEO_2-biotin and SrtA; lane 4: EGFP-LA, amine-PEO_2-biotin and SrtA; lane 5: EGFP-LA; lane 6: EGFP-LA, amine-PEO_2-biotin; lane 7: amine-PEO_2-biotin and SrtLp; lane 8: EGFP-LA, amine-PEO_2-biotin and SrtLp; M: molecular weight markers). (**C**) Western blot analysis of the products of the site-specific reaction between EGFP-LK and amine-PEO_2-biotin after sortase treatment (The arrows show confirmed protein modification. Lane 1: EGFP-LK; lane 2: EGFP-LK and amine-PEO_2-biotin; lane 3: amine-PEO_2-biotin and SrtA; lane 4: EGFP-LK, amine-PEO_2-biotin and SrtA; lane 5: EGFP-LK; lane 6: EGFP-LK, amine-PEO_2-biotin; lane 7: amine-PEO_2-biotin and SrtLp; lane 8: EGFP-LK, amine-PEO_2-biotin and SrtLp; M: molecular weight markers). (**D**) Western blot analysis of the products of the site-specific reaction between EGFP-LA and amine-PEO_2-biotin after sortase treatment (The arrows show confirmed protein modification. Lane 1: EGFP-LQ; lane 2: EGFP-LQ and amine-PEO_2-biotin; lane 3: amine-PEO_2-biotin and SrtA; lane 4: EGFP-LQ, amine-PEO_2-biotin and SrtA; lane 5: EGFP-LQ; lane 6: EGFP-LQ, amine-PEO_2-biotin; lane 7: amine-PEO_2-biotin and SrtLp; lane 8: EGFP-LQ, amine-PEO_2-biotin and SrtLp; M: molecular weight markers). Three independent experiments were carried out.

sortases only having TLXTC motif. High concentration of tagged-EGFP and amine PEO_2-biotin mixture might cause the high background, however, effective sortase reaction is required high substrate and sortase concentration [24], which should be improved.

Meanwhile, it should be noted that SrtA could not conjugate EGFP-LQ with amine-PEO_2-biotin, while SrtLp did conjugate EGFP-LQ and amine-PEO_2-biotin (Fig. 1D). SrtLp recognizes the LPQT-SEQ motif and can mediate conjugation of proteins with this motif with primary amines, although the substrate specificity of SrtA is restricted to proteins containing the LXXXG motif [25]. Therefore, we also examined the specificity of SrtLp or SrtA (data not shown) with other recognition sequences, as shown in Table 1. The results of western blot analysis of the reaction between tagged EGFP and amine-PEO_2-biotin after Srt treatment were summarized in Table 1. This experiment indicated that the substrate specificity of SrtLp is broader than that of SrtA. Although the yield of amine-modified protein was lower than previously reported [16], the different substrate specificity would be useful in protein engineering studies involving multi-labeling [19] or protein-immobilization [24, 26].

3.4 Sortase reaction with tagged EGFP and primary amine-modified particles

To expand the utility of SrtLp that can recognize the LPQTSEQ sequence and modify small molecules, we performed site-specific protein immobilization on primary amine-modified particles. SrtA or SrtLp reactions were performed between EGFP-LPKTG or EGFP-LPQTSEQ and primary amine-

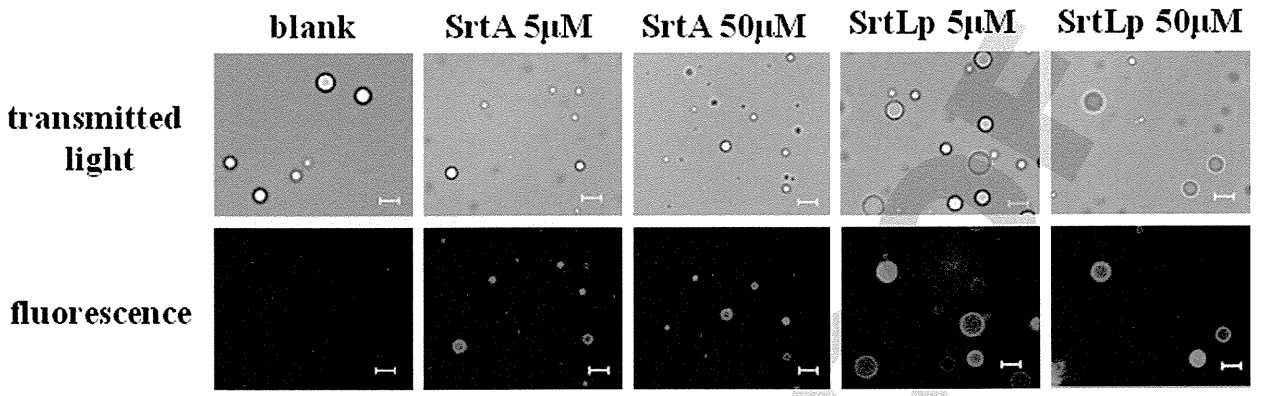

Figure 2. The sortase reaction product of amine-coated microbeads and tagged-EGFP were washed three times with PBS, dissolved PBS (20 μL), and directly observed using fluorescence microscopy. Microscopic analysis of the products of the site-specific reaction between tagged EGFP and amine-micromere particles after sortase treatment (scale bar = 10 μm). Three independent experiments were carried out.

modified particles, respectively. Although both SrtA and SrtLp could conjugate tagged EGFP to primary amine-modified particles, SrtLp much effectively conjugated tagged EGFP than SrtA (Fig. 2). These results were supported by previous reports that SrtA is not effectively conjugate between protein and primary amine [23]. Although the modification efficiency was lower than in cases involving the use of tri-glycine tags or other transglutaminases [25, 26], SrtLp allows immobilization of proteins with a different tag sequence.

4 Concluding remarks

We developed a novel sortase from *Lactobacillus plantarum* with different substrate specificity than *Staphylococcus aureus* sortase. Amine-directed protein modification was achieved using the SrtLp "LPQTSEQ" original recognition tag sequence, enabling us to perform direct protein conjugation on amine-modified particles. These results show that our method is a promising way to expand site-specific protein-small molecule modification.

This work was supported in part by a Grant-in-Aid for Young Scientist B (21760638) of Japan Society for the Promotion of Science (JSPS) and Special Coordination Funds for Promoting Science and Technology, Creation of Innovation Centers for Advanced Interdisciplinary Research Areas (Innovative Bioproduction Kobe), MEXT, Japan.

The authors declare no conflict of interest.

5 References

[1] Niemeyer, C. M., Bioorganic applications of semisynthetic DNA-protein conjugates. *Chem. A Eur. J.* 2001, *7*, 3189–3195.

[2] Niemeyer, C. M., The developments of semisynthetic DNA-protein conjugates. *Trends Biotech.* 2002, *20*, 395–401.

[3] Pelegrin, A., Folli, S., Buchegger, F., Mach, J. P. et al., Antibody-fluorescein conjugates for photoimmunodiagnosis of human colon carcinoma in nude mice. *Cancer* 1991, *67*, 2529–2537.

[4] Shimada, J., Maruyama, T., Hosogi, T., Tominaga, J. et al., Conjugation of DNA with protein using His-tag chemistry and its application to the aptamer-based detection system. *Biotech. Lett.* 2008, *30*, 2001–2006.

[5] Furukawa, H., Shimojyo, R., Ohonishi, N., Fukuda, H. et al., Affinity selection of target cells from cell surface displayed libraries: A novel procedure using thermo-responsive magnetic nanoparticles. *App. Micro. Biotech.* 2003, *62*, 478–483.

[6] Hoshino, A., Ohnishi, N., Yasuhara, M., Yamamoto, K. et al., Separation of murine neutrophils and macrophages by thermoresponsive magnetic nanoparticles. *Biotech. Prog.* 2007, *23*, 1513–1516.

[7] Lin, C. W., Ting, A. Y., Transglutaminase-catalyzed site-specific conjugation of small-molecule probes to proteins in vitro and on the surface of living cells, *J. Am. Chem. Soc.* 2006, *128*, 4542–4543.

[8] Mero, A., Spolaore, B., Veronese, F. M., Fontana, A., Transglutaminase-mediated PEGylation of proteins: direct identification of the sites of protein modification by mass spectrometry using a novel monodisperse PEG. *Bioconjug. Chem.* 2009, *20*, 384–389.

[9] Sato, H., Yamamoto, K., Hayashi, E., Takahara, Y., Transglutaminase-mediated dual and site-specific incorporation of poly(ethylene glycol) derivatives into a chimeric interleukin-2. *Bioconjug. Chem.* 2000, *11*, 502–509.

[10] Noda, S., Ito, Y., Shimizu, N., Tanaka, T. et al., Over-production of various secretory-form proteins in Streptomyces lividans. *Prot. Expr. Purif.* 2010, *73*, 198–202.

[11] Clancy, K. W., Melvin, J. A., McCafferty, D. G., Sortase transpeptidases: Insights into mechanism, substrate specificity, and inhibition. *Pept. Sci.* 2010, *94*, 385–396.

[12] Paterson, G. K., Mitchell, T. J., The biology of gram-positive sortase enzymes. *Trends Biotech.* 2004, *12*, 89–95.

[13] Zong, Y., Bice, T. W., Ton-That, H., Schneewind, O., Crystal structures of *Staphylococcus aureus* sortase A and its substrate complex. *J. Biol. Chem.* 2004, *279*, 31383–31389.

[14] Antos, J. M., Miller, G. M., Grotenbreg, G. M., Ploegh, H. L., Lipid modification of proteins through sortase-catalyzed transpeptidation. *J. Am. Chem. Soc.* 2008, *130*, 16338–16343.

[15] Matsumoto, T., Sawamoto, S., Sakamoto, T., Tanaka, T. et al., Site-specific tetrameric streptavidin-protein conjugation using sortase A. *J. Biotech.* 2011, *152*, 37–42.

[16] Sakamoto, T., Sawamoto, S., Tanaka, T., Fukuda, H. et al., Enzyme-mediated site-specific antibody-protein modification using a ZZ domain as a linker. *Bioconjug. Chem.* 2010, *21*, 2227–2233.

[17] Samantaray, S., Marathe, U., Dasgupta, S., Nandicoori, V. K. et al., Peptide-sugar ligation catalyzed by transpeptidase sortase: A facile approach to neoglycoconjugate synthesis. *J. Am. Chem. Soc.* 2008, *130*, 2132–2133.

[18] Antos, J., Popp, M. W., Ernst, R., Chew, G. et al., A straight path to circular proteins. *J. Biol. Chem.* 2009, *284*, 16028–16036.

[19] Antos, J., Chew, G., Guimaraes, C. P., Yoder, N. C. et al., Site-specific N- and C-terminal labeling of a single polypeptide using sortases of different specificity. *J. Am. Chem. Soc.* 2009, *131*, 10800–10801.

[20] Popp, M. W., Dougan, S. K., Chuang, T., Spooner, E. et al., Sortase-catalyzed transformations that improve the properties of cytokines. *Proc. Natl. Acad. Sci. USA* 2011, *108*, 3169–3174.

[21] Tanaka, T., Yamamoto, T., Tsukiji, S., Nagamune, T., Site-specific protein modification on living cells catalyzed by sortase. *ChemBioChem* 2008, *9*, 802–807.

[22] Ton-That, H., Liu, G., Mazmanian, S. K., Faul, K. F. et al., Purification and characterization of sortase, the transpeptidase that cleaves surface proteins of *Staphylococcus aureus* at the LPXTG motif. *Proc. Natl. Acad. Sci. USA* 1999, *96*, 12424–12429.

[23] Huang, X., Aulabaugh, A., Ding, W., Kapoor, B. et al., Kinetic mechanism of *Staphylococcus aureus* sortase SrtA. *Biochemistry* 2003, *42*, 11307–11315.

[24] Parthasarathy, R., Subramanian, S., Boder, E. T., Sortase A as a novel molecular "stapler" for sequence-specific protein conjugation. *Bioconjug. Chem.* 2007, *18*, 469–476.

[25] Kruger, R. G., Otvos, B., Frankel, B. A., Bentley, M. et al., Analysis of the substrate specificity of the *Staphylococcus aureus* sortase transpeptidase SrtA. *Biochemistry* 2004, *43*, 1541–1551.

[26] Moriyama, K., Sung, K., Goto, M., Kamiya, N., Immobilization of alkaline phosphatase on magnetic particles by site-specific and covalent cross-linking catalyzed by microbial transglutaminase. *J. Biosci. Bioeng.* 2011, *111*, 650–653.

Journal of Biotechnology 157 (2012) 124–129

Contents lists available at SciVerse ScienceDirect

Journal of Biotechnology

journal homepage: www.elsevier.com/locate/jbiotec

Protein-encapsulated bio-nanocapsules production with ER membrane localization sequences

Yuya Nishimura[a], Takuya Shishido[a], Jun Ishii[b], Tsutomu Tanaka[b], Chiaki Ogino[a], Akihiko Kondo[a,*]

[a] Department of Chemical Science and Engineering, Graduate School of Engineering, Kobe University, 1-1 Rokkodaicho, Nada-ku, Kobe 657-8501, Japan
[b] Organization of Advanced Science and Technology, Kobe University, Japan

ARTICLE INFO

Article history:
Received 11 July 2011
Received in revised form
14 September 2011
Accepted 16 September 2011
Available online 22 September 2011

Keyword:
Hepatitis B virus
Hepatitis B virus surface antigen
Drug delivery
Bio-nanocapsule
Encapsulation
Lipid modification

ABSTRACT

Bio-nanocapsules (BNCs) are hollow nanoparticles composed of the L protein of hepatitis B virus (HBV) surface antigen (HBsAg), which can specifically introduce genes and drugs into various kinds of target cells. Although the classic electroporation method has typically been used to introduce highly charged molecules such as DNA, it is rarely adopted for proteins due to its very low efficiency. In this study, a novel approach to the preparation of BNC was established whereby a target protein was pre-encapsulated during the course of nanoparticle formation. Briefly, because of the process of BNC formation in a budding manner on the endoplasmic reticulum (ER) membrane, the association of target proteins to the ER membrane with lipidation sequences (ER membrane localization sequences) could directly generate protein-encapsulating BNC in collaboration with co-expression of the L proteins. Since the membrane-localized proteins are automatically enveloped into BNCs during the budding event, this method can be protect the proteins and BNCs from damage caused by electroporation and obviate the need for laborious consideration to study the optimal conditions for protein encapsulation. This approach would be a useful method for encapsulating therapeutic candidate proteins into BNCs.

1. Introduction

Over the past couple of decades, drug delivery systems (DDS) have been intensively studied in order to improve the efficacy of chemotherapy and reduce its adverse effects. The delivery of bioactive molecules such as genes, chemical compounds and proteins to target cells is very significant for medical and biological applications (Nagai, 2005; Tabata, 2006). For this reason, it is necessary to establish an efficient carrier that ensures the internal stability of bioactive molecules, as well as their delivery into the targeted cells.

The bio-nanocapsule (BNC) is an attractive carrier for the delivery of bioactive molecules (Yamada et al., 2003). BNCs are hollow particles composed of the L protein of the hepatitis B virus (HBV), surface antigen (HBsAg), and the lipid bilayer derived from host cells (Kuroda et al., 1992). As carriers for drug delivery, these virus-like particles have many advantages, as follows: high specificity for human hepatocytes; high transfection efficiency, equivalent to the original HBV; reliable safety arising from the absence of the viral genome; high stability in the blood; and, a high capacity for encapsulation of genes and drugs (Yamada et al., 2003; Iwasaki et al., 2007; Jung et al., 2008).

To target cells other than hepatocytes, the specificity of BNC can be altered by genetic modifications. Varieties of specificity-altered BNCs have been produced by deleting the preS region having specificity for hepatocytes in the L protein, and inserting binding molecules targeting other cells (Kasuya et al., 2008, 2009). Antibodies and peptides have often been selected as such affinity molecules. To confer specificity for various kinds of cell surface receptors, antibody-mediated targeting with the ZZ domain (derived from protein A) or with biotin, which binds to the Fc region of immunoglobulin G (IgG) or streptavidin, has been developed as a practical and versatile technique (Iijima et al., 2011; Shishido et al., 2009a). Similarly, affibody molecules, which comprise a new class of affinity ligands derived from the Z domain and bind a range of different proteins, e.g. insulin, HER2 and EGFR, were used as a substitute for antibodies, while an arginine-rich peptide was displayed on BNC to permit the delivery into various types of cells (Nygren, 2008; Shishido et al., 2009b).

Abbreviations: DDS, drug delivery system; BNC, bio-nanocapsule; HBV, hepatitis B virus; HBsAg, hepatitis B virus surface antigen; ER, endoplasmic reticulum; IgG, immunoglobulin G; HER2, human EGFR-related 2; EGFR, epidermal growth factor receptor; MLS, membrane localization sequence; EGFP, enhanced green fluorescent protein; PCR, polymerase chain reaction; PEG, polyethylene glycol; PBS, phosphate-buffered saline; CsCl, discontinuous cesium chloride; EDTA, ethylene diamine tetraacetic acid; EIA, enzyme immunoassay; SDS-PAGE, sodium dodecyl sulphate-polyacrylamide gel electrophoresis electrotransferred onto a; PVDF, polyvinilidene fluoride; AP, alkaline phosphatase; BCIP, 5-bromo-4-chloro-3-indolyl phosphate; NBT, nitro blue tetrazolium; DLS, dynamic light scattering.

* Corresponding author. Tel.: +81 78 803 6196; fax: +81 78 803 6196.
E-mail address: akondo@kobe-u.ac.jp (A. Kondo).

0168-1656/$ – see front matter © 2011 Elsevier B.V. All rights reserved.
doi:10.1016/j.jbiotec.2011.09.015

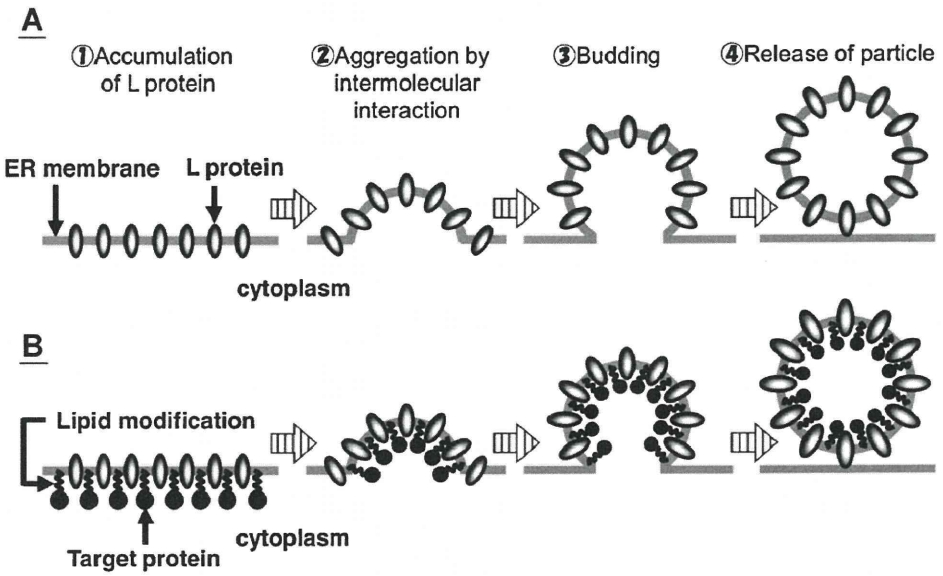

Fig. 1. Schematic illustration for the process of BNC formation in insect cells. (A) A common process of BNC formation. Translated L proteins are accumulated on the ER membrane and aggregated by intermolecular interaction. Hollow particles are released via budding events by self-assembly into the side of the ER lumen. (B) A strategy for direct production of protein-encapsulating BNC. Since target proteins are localized on the ER membrane by lipid modification, they are easily encapsulated inside BNC through the same process of common particle formation.

As described above, BNCs are useful carriers to deliver drugs specifically to different cell types. However, methods to encapsulate drugs into BNC have not been studied extensively. Therefore, the classic electroporation method is commonly used for this purpose (Yamada et al., 2003). Besides expensive equipment, this method requires consideration of the appropriate conditions that affect the encapsulation efficiency through various factors such as the intensity of electric voltage and pulse, temperature, concentration of particles and drugs, and composition of buffers (Yamada et al., 2003). Although electroporation has typically been used to introduce highly charged molecules such as DNA, it is rarely adopted for proteins due to its very low efficiency. Furthermore, many proteins, including pharmaceutical proteins, might suffer serious damage from high voltage, because they have a tendency to be denatured and agglutinated under severe conditions such as pH, heat and concentration (Chi et al., 2003). Thus, a simple and effective method for encapsulating proteins into BNC without using electroporation is needed.

In the present study, a novel approach to the preparation of BNC was established, in which a target protein is pre-encapsulated in the course of particle formation. We focused on the following mechanism for the formation of BNC (Fig. 1A): (1) L proteins localize and accumulate on the ER membrane; (2) aggregation of the L proteins is initiated by the accumulated L proteins on the ER; (3) intermolecular interactions trigger budding of the L particles; and, (4) hollow particles are formed within the ER lumen by a nucleocapsid-independent extrusion process and then exported from the cells via the vesicular transport pathway (Kuroda et al., 1992). BNC is thus produced when budding forms on the ER membrane. Therefore, the working assumption in the present study was that co-expression of the target proteins with the L proteins that associate with the outer leaflet of the ER membrane (cytoplasm side) by lipid modification could encapsulate the target proteins into the BNC, and would be accompanied by the formation of particles (Fig. 1B). As a means for this approach, lipidation sequences (membrane localization sequences; MLSs) derived from N-Ras, which cause prenylation in the CAAX motif (Choy et al., 1999), were added to the C-terminal of the target proteins. Since the ER membrane-localized target proteins were automatically embedded in the BNC during the formation process, this approach never required laborious consideration of the electroporation conditions after the preparation of hollow BNC particles, despite procedures identical to the previous process for the production and purification of BNC. We verified the feasibility of this strategy to encapsulate the target proteins into the BNC with lipidation motifs.

2. Materials and methods

2.1. Construction of plasmids for the expression of membrane-localized proteins in insect cells

MLS1 and MLS2 derived from N-Ras were selected as the lipidation sequences (Sato et al., 2006). The plasmids for expression of the enhanced green fluorescent protein (EGFP), attached with MLS1 or MLS2 in insect cells, were constructed as described below (Fig. 2A). The fragments encoding the EGFP-MLS1 or EGFP-MLS2 fusion gene were amplified by polymerase chain reaction (PCR) from pEGFP (Takara Bio, Shiga, Japan) with the following primers: EGFP-MLS1 (5′-GGGGGATCCATGGTGAGCAAGGGCGAGGA-3′ and 5′-GGGCCGC GGTTACATCACCACGCAGGGCAGGCCCATGCAGCCCTGCTTGTACAGC TCGTCCATGC-3′) and EGFP-MLS2 (5′-GGGGGATCCATGGTGAGCA AGGGCGAGGA-3′ and 5′-GGGCCGCGGTTACATCACCACGCAGGGCA GGCCCATGGAGCCCTGCTTGTACAGCTCGTCCATGC-3′). The amplified fragments were digested with *Bam*HI/*Sac*II and ligated into the pXIHAbla (Shishido et al., 2009c) (Fig. 2B). The resulting plasmids were designated as pXIHAbla-EGFP-MLS1 and pXIHAbla-EGFP-MLS2. The previously constructed plasmid pXIHAbla-EGFP (Shishido et al., 2009c) was used for the expression of cytosolic EGFP in a comparative expression manner. In contrast, plasmid pX-ML (Shishido et al., 2006) was used for the co-expression of BNC with these plasmids in insect cells (Fig. 2C).

2.2. Transfection of plasmids for the expression of EGFP-MLSs and/or BNC

A *Trichoplusia ni* BTI-TN-5B1-4 insect cell line (High Five) (Invitrogen, Carlsbad, CA, USA) was maintained in a serum-free medium (Express Five SFM) (Invitrogen) supplemented with 0.26 g/L

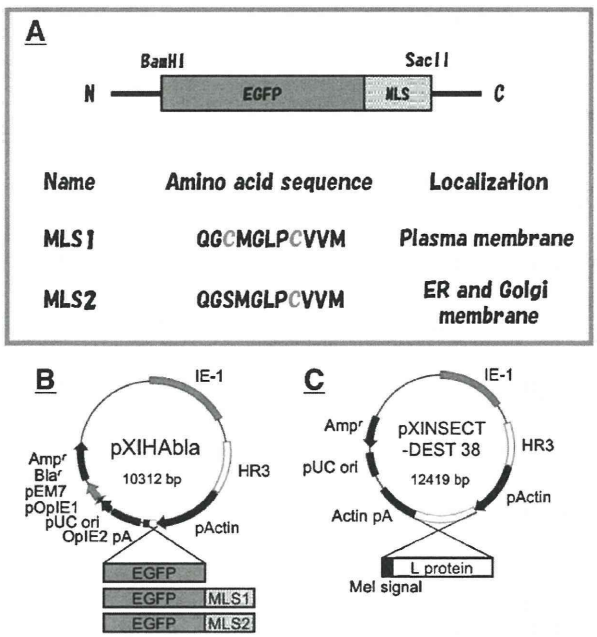

Fig. 2. Schematic representation of constructs to localize target proteins on the ER membrane of insect cells. ER membrane-localized proteins would be easily encapsulated into BNCs. (A) EGFP was used as a model for the target proteins. MLS1 and MLS2 derived from N-Ras were reported to localize on plasma or on the ER membrane in mammalian cells. Gray characters indicate the amino acid residues involved in lipid modifications. (B) Insect cell shuttle vector for expression of EGFP, EGFP-MLS1 and EGFP-MLS2. (C) Expression vector for secretion of BNC in insect cells.

L-glutamine and 10 mg/L gentamicin (Invitrogen) at 27 °C. High Five cells were seeded on a 35 mm dish at a density of 2×10^5 cells/ml for 24 h before transfection, and the cells were then used for transfection.

For observation by confocal laser scanning microscopy, the EGFP expression plasmid (pXIHAbla-EGFP, pXIHAbla-EGFP-MLS1 or pXIHAbla-EGFP-MLS2) was transfected into the High Five cells using FuGENE HD transfection reagent (Roche, Basel, Switzerland), following the manufacturer's procedure.

For purification of BNCs, pX-ML and EGFP expression plasmid (pXIHAbla-EGFP, pXIHAbla-EGFP-MLS1 or pXIHAbla-EGFP-MLS2) were co-transfected into High Five cells using FuGENE HD transfection reagent.

2.3. Confocal laser scanning microscopy observation of EGFP localization in insect cells

At 72 h after transfection, the cells were observed with a laser-scanning confocal microscope (Carl Zeiss, Oberkochen, Germany), following the manufacturer's procedure. Fluorescence images were acquired using the 488 nm line of an Ar laser for excitation and a 505 nm band pass filter for emission. The specimens were viewed using a 63-fold oil immersion objective.

2.4. Expression and purification of BNCs co-expressed with EGFP-MLSs

At 72 h after transfection, the culture supernatant (20 ml) of transfected insect cells was collected and mixed with polyethylene glycol (PEG) 6000 solution (33%, w/v). After 2 h incubation, the mixture was centrifuged at 10,000 × *g* for 30 min at 4 °C and the precipitate was dissolved in 2.8 ml of phosphate-buffered saline (PBS). The solution was layered onto a discontinuous cesium chloride (CsCl) gradient (11 ml, concentration: 10–40% (w/v) in buffer A [0.1 M sodium phosphate, 15 mM ethylene diamine tetraacetic acid (EDTA)]) and centrifuged at 24,000 rpm for 16 h at 15 °C in a himac CP70MXX centrifuge equipped with swing roter P40ST (Hitachi, Tokyo, Japan). The amount of BNC in each fraction was analyzed using an IMx enzyme immunoassay (EIA) kit (Abbott Laboratories, Abbott Park, IL, USA), following the manufacturer's procedure, and BNC was dialyzed against PBS. After dialysis, the BNC solution was layered onto a discontinuous sucrose gradient (11 ml, concentration: 10–50% (w/v) in buffer A) and centrifuged at 24,000 rpm for 10 h at 4 °C. The amount of BNC in each fraction was determined using the IMx EIA kit, and the expression of EGFP was confirmed by western blotting. Fractions containing BNC were dialyzed against PBS and stored at 4 °C.

2.5. SDS-PAGE and western blotting

The expression of EGFP in each fraction was confirmed by western blotting. The supernatant was fractionated by sodium dodecyl sulphate-polyacrylamide gel electrophoresis (SDS-PAGE) and electrotransferred onto a polyvinilidene fluoride (PVDF) membrane. Rabbit anti-EGFP antibodies (Medical Biological Laboratories, Nagoya, Japan) were used for immunoblotting, followed by anti-rabbit antibodies conjugated with alkaline phosphatase (AP) (Promega, Madison, WI, USA). The membrane was stained with 5-bromo-4-chloro-3-indolyl phosphate (BCIP) and nitro blue tetrazolium (NBT) (Promega).

2.6. Dynamic light scattering analysis of purified BNCs co-expressed with EGFP-MLSs

The size of the purified BNCs co-expressed with EGFP-MLSs was determined by dynamic light scattering (DLS) using a Zetasizer Nano particle size analyzer (Malvern Instruments Ltd., Worcestershire, UK), following the manufacturer's procedure.

3. Results and discussion

3.1. Strategy for direct production of protein-encapsulating BNC

The aim of the present study was to establish a novel approach that would enable the simple preparation of protein-encapsulating BNC. Because BNC is produced by a bioprocess, we hypothesized that BNC that inherently encapsulated the protein drug candidates could be prepared with genetic modifications. If protein-encapsulating BNC could be produced by the same process that is commonly used for preparing hollow BNC particles, this would permit the protection of BNC and proteins from damage caused by electroporation and obviate the need for laborious efforts to study the optimal conditions for protein encapsulation.

For these reasons, we focused on the formation mechanism of BNC, that is, budding on the ER membrane, as shown in Fig. 1A (Kuroda et al., 1992). We assumed that the co-expression of target proteins on the ER membrane might directly generate protein-encapsulating BNC by enveloping the membrane-localized proteins during the budding event (Fig. 1B). The strategy used to test the feasibility of this approach was to introduce MLSs into the C-terminus of the target proteins. Two types of peptide motifs, 11-amino-acid sequences derived from N-Ras including the CAAX motif, were selected as the MLSs for the lipidation. MLS1 (QGCMGLPCVVM) is lipidated through both prenylation at the cysteine residue on the CAAX motif and palmitoylation at the upstream cysteine residue (Choy et al., 1999) (Fig. 2A). However, MLS2 (QGSMGLPCVVM) is lipidated by only prenylation at the cysteine residue on the CAAX motif, since the Cys3 of MLS1 is replaced with a serine residue (Choy et al., 1999) (Fig. 2A). According to the literature, MLS1 was localized to the plasma membrane, and MLS2 was localized to the ER

membrane and golgi membrane apparatus in mammal cells (Sato et al., 2006). For the present study, an insect cell allowing secretory production of BNC (Shishido et al., 2006) was used as the host cell, and EGFP was used as the model target protein, which facilitated the evaluation of both localization and encapsulation of BNC.

3.2. Localization of target proteins with membrane localization sequences (MLSs) in insect cells

To confirm whether MLSs have ER membrane localization abilities in insect cells, plasmids were constructed expressing EGFP, EGFP-MLS1, and EGFP-MLS2 (Fig. 2B). These three types of plasmids were transfected into insect cells (High Five) without the plasmid producing BNC, and their localization was observed with a confocal laser-scanning microscope (Fig. 3).

Because of its lack of membrane localization ability, EGFP without MLS was observed in the cytoplasm of insect cells. EGFP-MLS1 was evenly localized on the plasma and ER membranes in insect cells, although MLS1 reportedly locates on the plasma membrane in mammal cells. In contrast, EGFP-MLS2 was strongly but partially localized to the ER membrane. Thus, in the present study, both MLS1 and MLS2 functioned as membrane localization sequences in insect cells and had the capacity to localize EGFP on ER membranes, even though they varied in their ER localization ability. This result indicates that both MLS1 and MLS2 are capable of localizing target proteins on an ER membrane as therapeutic candidates in a similar fashion.

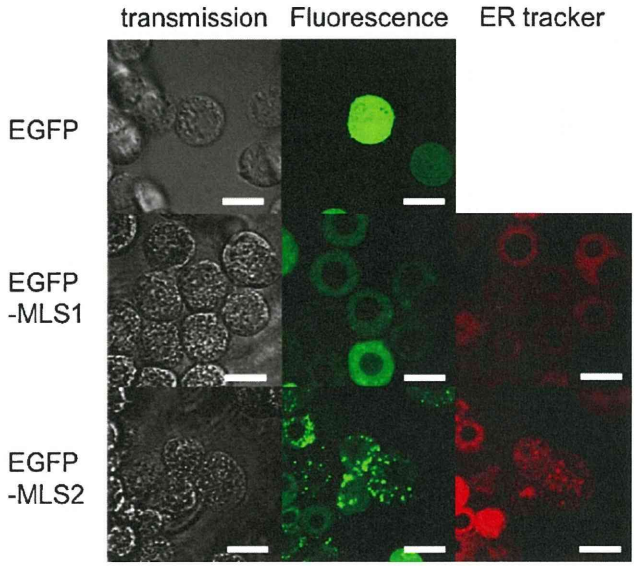

Fig. 3. Fluorescence images for observation of the localization of EGFP in insect cells with confocal microscopy. ER-tracker (Invitrogen) was used as the localization marker. The upper images are the cells transfected with EGFP expression plasmid. The middle images are the cells transfected with EGFP-MLS1 expression plasmid. The lower images are the cells transfected with EGFP-MLS2 expression plasmid. Scale bars; 20 μm.

3.3. Production and purification of EGFP-encapsulating BNC

To investigate the validity of our approach, the three types of plasmids (for expression of EGFP, EGFP-MLS1 and EGFP-MLS2) were co-transfected, with the plasmid producing BNC, into insect cells (High Five). After 72 h of cultivation, the supernatants were harvested and the BNCs were purified by gradient ultracentrifugation, as described in materials and methods. The resultant fractions were analyzed by EIA to measure the amount of BNC and by western blotting to evaluate whether the BNCs encapsulated EGFP (Fig. 4). After dialysis, about 25 μg of purified EGFP-MLS1/BNC

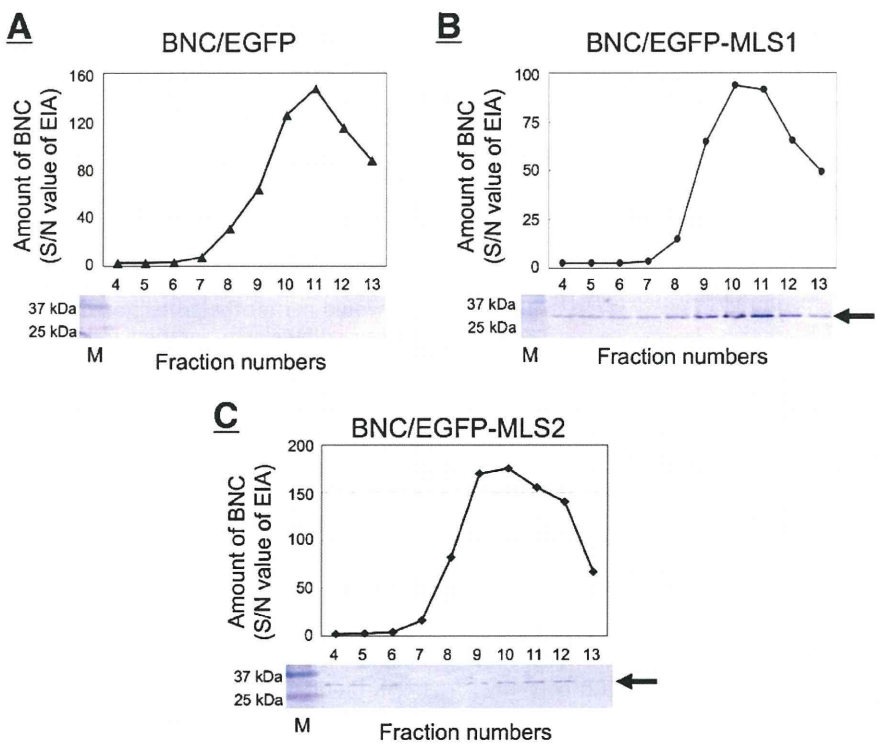

Fig. 4. Examination for encapsulation of EGFP into the purified BNCs. After sucrose gradient centrifugation, the amount of BNC including each fraction was measured with an IMx EIA kit (S/N value of EIA). The same fractions were tested for the presence of EGFP by western blotting with anti-EGFP antibody. Co-expression of (A) BNC and EGFP, (B) BNC and EGFP-MLS1, and (C) BNC and EGFP-MLS2.

Table 1
Purification summary of EGFP-MLS1/BNC and EGFP-MLS2/BNC.

Sample name	Step	Volume (ml)	Concentration (μg/ml)	Mass (μg)
EGFP-MLS1/BNC	Culture medium supernatant	20.0	2764.8	55,296.6
	Pellet after PEG settling method	2.8	1220.0	3416.0
	After CsCl ultracentrifugal method	3.0	54.9	164.6
	After Sucrose ultracentrifugal method	6.0	3.2	19.4
	After concentration	0.5	51.6	25.8
EGFP-MLS2/BNC	Culture medium supernatant	20.0	2683.6	53,672.3
	Pellet after PEG settling method	2.8	726.2	2033.3
	After CsCl ultracentrifugal method	3.0	58.1	174.3
	After Sucrose ultracentrifugal method	6.0	6.5	38.7
	After concentration	0.7	35.5	24.9

and EGFP-MLS2/BNC were obtained from 20 ml of culture medium supernatant (Table 1).

First, in the case of co-transfection of EGFP and BNC, although the main peaks of BNCs appeared in 10–12 fractions, the bands of EGFP were not detected in the same fractions (Fig. 4A). This result indicates that EGFP was not encapsulated in BNC, although BNC was produced uneventfully in the insect cells. Second, in the case of co-transfection of EGFP-MLS1 and BNC, the thick bands of EGFP were detected in 9–12 fractions, which displayed the main peaks of BNC (Fig. 4B). This suggests that EGFP-encapsulating BNC was successfully produced by introduction of the MLS1 motif. In the third case, co-transfection of EGFP-MLS2 and BNC displayed a result similar to the case of EGFP-MLS1 and BNC (Fig. 4C), suggesting that the introduction of MLS2 also allowed the production of EGFP-encapsulating BNC. The smaller amounts of EGFP in the BNC with MLS2 might be attributed to partial localization on the ER. However, since the EGFP-encapsulating BNC with MLS2 produced almost twice the amount of particles as that with MLS1, this suggests that MLS2 might be a better expression system for protein-encapsulating BNC (Fig. 4B and 4C). These differences might be due to the presence or absence of the palmitoylation site between MLS1 and MLS2.

Finally, the diameters of the BNC particles were evaluated using the DLS method (Fig. 5). The diameters of the three types of particles were almost equivalent, at 150 nm, indicating that the diameter of EGFP-encapsulating BNCs was similar to that of hollow BNC particles produced in insect cells (Kurata et al., 2008). In addition, it was also confirmed that the EGFP-encapsulating BNCs kept the targeting abilities to human hepatocytes (Supplementary Fig. 1).

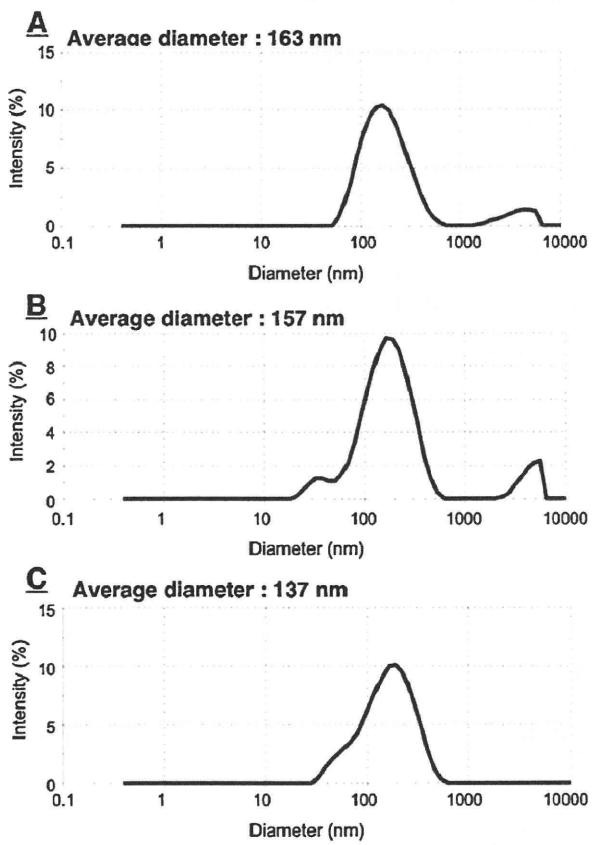

Fig. 5. DLS analyses of purified BNCs. Co-expression of (A) BNC and EGFP, (B) BNC and EGFP-MLS1, and (C) BNC and EGFP-MLS2.

4. Conclusions

The feasibility of this approach to the direct production of protein-encapsulating BNC by localizing the target proteins on the ER membrane was successfully demonstrated. In this study, MLS1 and MLS2 of N-Ras were used to localize the target proteins on the ER membrane either by prenylation or by palmitoylation. While MLS1 and MLS2 could incorporate our approach, other ER membrane localization sequences with different modification mechanisms might also be utilized to produce protein-encapsulating BNCs. In addition, whereas therapeutic candidate proteins might be encapsulated in BNC in the same manner as EGFP, this should be demonstrated in the near future. This approach would be a useful tool for encapsulating target proteins into BNCs.

Acknowledgements

This work was partially supported by a Special Coordination Fund for Promoting Science and Technology, Creation of Innovative Centers for Advanced Interdisciplinary Research Areas (Innovative Bioproduction Kobe) from the Ministry of Education, Culture, Sports and Technology (MEXT), and Science Research Grants from the Ministry of Health, Labor and Welfare, Japan.

Appendix A. Supplementary data

Supplementary data associated with this article can be found, in the online version, at doi:10.1016/j.jbiotec.2011.09.015.

References

Nagai, T., 2005. Drug discovery and innovative drug delivery research in new drug development. Pharm. Tech. Jpn. 21, 1949–1951.
Tabata, T., 2006. Drug delivery system: basic technology for biomedical research, medical treatment and health care. Biotechnol. J. 6, 553–555.
Yamada, T., Iwasaki, Y., Tada, H., Iwabuki, H., Chuah, M.K., VandenDriessche, T., Fukuda, H., Kondo, A., Ueda, M., Seno, M., Tanizawa, K., Kuroda, S., 2003. Nanoparticles for the delivery of genes and drugs to human hepatocytes. Nat. Biotechnol. 21, 885–890.

Kuroda, S., Otaka, S., Miyazaki, T., Nakao, M., Fujisawa, Y., 1992. Hepatitis B virus envelope L protein particles. Synthesis and assembly in *Saccharomyces cerevisiae*, purification and characterization. J. Biol. Chem. 267, 1953–1961.

Iwasaki, Y., Ueda, M., Yamada, T., Kondo, A., Seno, M., Tanizawa, K., Kuroda, S., Sakamoto, M., Kitajima, M., 2007. Gene therapy of liver tumors with human liver-specific nanoparticles. Cancer Gene Ther. 14, 74–81.

Jung, J., Matsuzaki, T., Tatematsu, K., Okajima, T., Tanizawa, K., Kuroda, S., 2008. Bio-nanocapsule conjugated with liposomes for in vivo pinpoint delivery of various materials. J. Control. Release 126, 255–264.

Kasuya, T., Jung, J., Kadoya, H., Matsuzaki, T., Tatematsu, K., Okajima, T., Miyoshi, E., Tanizawa, K., Kuroda, S., 2008. In vivo delivery of bionanocapsules displaying phaseolus vulgaris agglutinin-L_4 isolectin to malignant tumors overexpressing N-acetylglucosaminyltransferase V. Hum. Gene Ther., 887–895.

Kasuya, T., Jung, J., Kinoshita, R., Goh, Y., Matsuzaki, T., Iijima, M., Yoshimoto, N., Tanizawa, K., Kuroda, S., 2009. Bio-nanocapsule–liposome conjugates for in vivo pinpoint drug and gene delivery. Methods Enzymol. 464, 147–166.

Iijima, M., Kadoya, H., Hatahira, S., Hiramatsu, S., Jung, G., Martin, A., Quinn, J., Jung, J., Jeong, S.Y., Choi, E.K., Arakawa, T., Hinako, F., Kusunoki, M., Yoshimoto, N., Niimi, T., Tanizawa, K., Kuroda, S., 2011. Nanocapsules incorporating IgG Fc-binding domain derived from *Staphylococcus aureus* protein A for displaying IgGs on immunosensor chips. Biomaterials 32, 1455–1464.

Shishido, T., Azumi, Y., Nakanishi, T., Umetsu, M., Tanaka, T., Ogino, C., Fukuda, H., Kondo, A., 2009a. Biotinylated bionanocapsules for displaying diverse ligands toward cell-specific delivery. J. Biochem. 146, 867–874.

Nygren, P.A., 2008. Alternative binding proteins: affibody binding proteins developed from a small three-helix bundle scaffold. FEBS J. 275, 2668–2676.

Shishido, T., Yonezawa, D., Iwata, K., Tanaka, T., Ogino, C., Fukuda, H., Kondo, A., 2009b. Construction of arginine-rich peptide displaying bionanocapsules. Bioorg. Med. Chem. Lett. 19, 1473–1476.

Chi, E.Y., Krishnan, S., Randolph, T.W., Carpenter, J.F., 2003. Physical stability of proteins in aqueous solution: mechanism and driving forces in nonnative protein aggregation. Pharm. Res. 20, 1325–1336.

Choy, E., Chiu, V.K., Silletti, J., Feoktistov, M., Morimoto, T., Michaelson, D., Ivanov, I.E., Philips, M.R., 1999. Endomembrane trafficking of ras: the CAAX motif targets proteins to the ER and Golgi. Cell 98, 69–80.

Sato, M., Ueda, Y., Umezawa, Y., 2006. Imaging diacylglycerol dynamics at organelle membranes. Nat. Methods 3, 797–799.

Shishido, T., Kurata, N., Yoon, M.E., Tanaka, T., Yamaji, H., Fukuda, H., Kondo, A., 2009c. A high-level expression vector containing selectable marker for continuous production of recombinant protein in insect cells. Biotechnol. Lett. 31, 623–627.

Shishido, T., Muraoka, M., Ueda, M., Seno, M., Tanizawa, K., Kuroda, S., Fukuda, H., Kondo, A., 2006. Secretory production system of bionanocapsules using a stably transfected insect cell line. Appl. Microbiol. Biotechnol. 73, 505–511.

Kurata, N., Shishido, T., Muraoka, M., Tanaka, T., Ogino, C., Fukuda, H., Kondo, A., 2008. Specific protein delivery to target cells by antibody-displaying bionanocapsules. J. Biochem. 144, 701–707.

Ultrasonics Sonochemistry 19 (2012) 607–614

Contents lists available at SciVerse ScienceDirect

Ultrasonics Sonochemistry

journal homepage: www.elsevier.com/locate/ultsonch

Targeted sonodynamic therapy using protein-modified TiO_2 nanoparticles

Kazuaki Ninomiya [a], Chiaki Ogino [b], Shuhei Oshima [c], Shiro Sonoke [c], Shun-ichi Kuroda [d], Nobuaki Shimizu [a,*]

[a] Institute of Nature and Environmental Technology, Kanazawa University, Kanazawa 920-1192, Japan
[b] Department of Chemical Science and Engineering, Graduate School of Engineering, Kobe University, Kobe 657-8501, Japan
[c] Division of Material Engineering, Graduate School of Natural Science and Technology, Kanazawa University, Kanazawa 920-1192, Japan
[d] Department of Bioengineering Sciences, Graduate School of Bioagricultural Sciences, Nagoya University, Nagoya 464-8601, Japan

ARTICLE INFO

Article history:
Received 13 August 2011
Received in revised form 13 September 2011
Accepted 22 September 2011
Available online 4 October 2011

Keywords:
Ultrasound
Titanium dioxide
Nanoparticles
Pre-S1/S2
Sonodynamic therapy

ABSTRACT

Our previous study suggested new sonodynamic therapy for cancer cells based on the delivery of titanium dioxide (TiO_2) nanoparticles (NPs) modified with a protein specifically recognizing target cells and subsequent generation of hydroxyl radicals from TiO_2 NPs activated by external ultrasound irradiation (called TiO_2/US treatment). The present study first examined the uptake behavior of TiO_2 NPs modified with pre-S1/S2 (model protein-recognizing hepatocytes) by HepG2 cells for 24 h. It took 6 h for sufficient uptake of the TiO_2 NPs by the cells. Next, the effect of the TiO_2/US treatment on HepG2 cell growth was examined for 96 h after the 1 MHz ultrasound was irradiated (0.1 W/cm^2, 30 s) to the cells which incorporated the TiO_2 NPs. Apoptosis was observed at 6 h after the TiO_2/US treatment. Although no apparent cell-injury was observed until 24 h after the treatment, the viable cell concentration had deteriorated to 46% of the control at 96 h. Finally, the TiO_2/US treatment was applied to a mouse xenograft model. The pre-S1/S2-immobilized TiO_2 (0.1 mg) was directly injected into tumors, followed by 1 MHz ultrasound irradiation at 1.0 W/cm^2 for 60 s. As a result of the treatment repeated five times within 13 days, tumor growth could be hampered up to 28 days compared with the control conditions.

1. Introduction

Ultrasound has been widely utilized for medical diagnosis due to its ability to penetrate tissue with less attenuation of energy. Ultrasound is also applied to therapeutic use, typically for cancer therapy [1]. There are two uses for ultrasound in cancer therapy. One is for hyperthermic cancer therapy based on the thermal effect of high-intensity focused ultrasound [2]. The other is sonodynamic cancer therapy based on non-thermal and sonochemical effects from the combination of low-intensity ultrasound and sonosensitizer (e.g. anti-cancer drugs or certain chemicals) which exhibit the preferential uptake and/or accumulation in tumor tissues and subsequent activation by ultrasound irradiation [3–5]. In 1989, Umemura et al. [6] suggested sonodynamic therapy (SDT) for cancer cells using hematoporphyrin, formally known as a photosensitizer for photodynamic therapy (PDT) [7], since the clinical application of PDT is very limited to cancer at the surface region due to the inability of photo energy to penetrate deep tissues.

Titanium dioxide (TiO_2) has been generally known as photocatalyst, generating reactive oxygen species (ROS) under ultraviolet irradiation [8,9]. The ROS produced by the photocatalytic effect of TiO_2 particles has been applied to killing cancer cells [10–12] as well as the degradation of harmful chemicals and inactivation of microorganisms. From the viewpoint of practical application, some groups demonstrated that nanoparticles (NPs) of TiO_2 could be used as a photocatalyst for injuring cancer cells [13–16]. Moreover, it was reported that the surface of TiO_2 NPs was modified with antibody recognizing cancer cells in order to localize the ROS effect toward the targeted cells, and that the antibody-immobilized TiO_2 NPs could be used for the photocatalytic injury of cancer cells [17–19]. However, the problem of the superficially-limited therapeutic effect would remain as long as these kinds of TiO_2 photocatalysts are activated by photo-energy, like the photosensitizer in the PDT.

Recently, our group discovered that TiO_2 could act as a sonocatalyst; namely, the presence of TiO_2 particles could enhance the hydroxyl (OH) radical generation by ultrasound irradiation even in the dark without ultraviolet irradiation [20]. The sonocatalytic effect of TiO_2 (nano)particles has been applied to degradation of certain kinds of chemicals [21,22], and inactivation of microorganisms [23–26]. With regard to the application of the sonocatalytic effect of TiO_2 NPs on cancer cell injury, our previous study first demonstrated that TiO_2 NPs modified with a targeting protein could be incorporated in cancer cells, and activated sonocatalytically to generate OH radicals, resulting in damage to the cell membrane [27]. Recently, some groups also reported *in vitro* and *in vivo* SDT using

* Corresponding author. Tel.: +81 76 234 4807; fax: +81 76 234 4829.
E-mail address: nshimizu@t.kanazawa-u.ac.jp (N. Shimizu).

1350-4177/$ - see front matter © 2011 Elsevier B.V. All rights reserved.
doi:10.1016/j.ultsonch.2011.09.009

the TiO_2 NPs as a sonocatalyst [28,29]. However, these reports did not examine the detailed kinetics of TiO_2 NPs uptake by the cancer cells and the prolonged effect of SDT using the TiO_2 NPs on the cell viability *in vitro*.

Therefore, in the present study, the efficacy of the SDT using protein-immobilized TiO_2 NPs (called TiO_2/US treatment) was examined *in vitro* and *in vivo*. This study specifically examines the uptake behavior of TiO_2 NPs modified with pre-S1/S2 (part of the L protein from the hepatitis B virus with high affinity to hepatocyte [30]) by HepG2 cells. Moreover, this study examines the effect of the TiO_2/US treatment on apoptosis induction in the early stage and the subsequent growth behavior of cancer cells. Lastly, the TiO_2/US treatment was tested *in vivo* using a mouse xenograft model.

2. Materials and methods

2.1. Pre-S1/S2-immobilized TiO_2 NPs

Suspension of TiO_2 NPs (MPT-422, Ishihara Sangyo Kaisha, Ltd., Osaka, Japan) was used as starting materials for preparing Pre-S1/S2-immobilized TiO_2 NPs. The recombinant fusion proteins GST-GFP and GST-GFP-pre-S1/S2 were prepared using *Escherichia coli* BL21(DE3) harboring plasmid pGEX-GFP or pGEX-GFP-pre-S1/S2 [31] as per the procedure described previously [27]. The chemicals used in this study were of guaranteed reagent grade without further purification.

Surface of the TiO_2 NPs was modified by polyacrylic acids (PAA) as described previously to avoid aggregation of TiO_2 NPs under physiologic conditions [32]. The GST-GFP or GST-GFP-pre-S1/S2 protein was immobilized on the surface of the PAA-modified TiO_2 NPs by chemical coupling at the carboxyl residue, using 1-ethyl-3-(3-dimethylaminopropyl) carbodiimide hydrochloride and *N*-hydroxysuccinimide (Wako Pure Chemical Industries, Osaka, Japan) [27,32]. The resultant NPs (120 nm in average size [27]) were designated as GFP-TiO_2 NPs and pre-S1/S2-GFP-TiO_2 NPs, respectively, in the present study.

2.2. Cell culture and animals

Human hepatoma HepG2 cells were used as model cancer cells throughout the study. When necessary, human colon carcinoma cells WiDr were also used. The HepG2 cells were cultured in Dulbecco's modified Eagle medium (DMEM, Nakarai Tesqu, Kyoto, Japan) supplemented with 10% (v/v) fetal bovine serum (FBS; Invitrogen GIBCO, Carlsbad, CA, USA), 60 μg/ml penicillin (Nakarai Tesqu, Kyoto, Japan), and 100 μg/ml streptomycin (Nakarai Tesqu, Kyoto, Japan). The cells were maintained at 37 °C and under a 5% CO_2 atmosphere.

BALB/c nude mice were used to prepare the xenograft model. The mice were housed in a controlled environment at 22 °C on 12 h light/dark cycles. The mice were 5 weeks old at the beginning of the experiments, weighing 22–25 g. The experimental animals were treated according to the standards supported by the animal protection committee of Kanazawa University.

2.3. TiO_2/US treatment in vitro

For the *in vitro* experiments, 4×10^5 HepG2 cells suspended in 2 ml DMEM were seeded in 35-mm culture dishes and incubated for 24 h. The pre-S1/S2-GFP-TiO_2 NPs suspension was added to the culture medium at a final concentration of 0.01% (w/v) and incubated for an additional 0–24 h. Pre-S1/S2 mediated uptake of the TiO_2 NPs by HepG2 cells were separately evaluated as described below. After additional incubation, the culture dishes were washed three times with fresh DMEM to remove the floating TiO_2 NPs, and finally the washed culture dishes were supplemented with 2 ml of fresh DMEM. The culture dish was placed on the transducer of the ultrasonic apparatus (Sonic Master ES-2, OG Giken Co., Ltd., Okayama, Japan) after the surface of the transducer was covered with 3 ml of water. Ultrasound was then irradiated from the bottom of the dishes under the following condition: frequency, 1 MHz; duty ratio, 50%; output power: 0.1 W/cm^2; and irradiation time, 30 s. After the TiO_2/US treatment, the dishes were incubated for 96 h. The culture medium was renewed at 48 h after the treatment. The viable cell number and apoptosis of HepG2 cells were evaluated at the prescribed time points.

2.4. TiO_2/US treatment in vivo

For the *in vivo* experiments using the mouse xenograft model, the HepG2 cells suspension in PBS (2×10^7 cells/ml) were mixed with one volume of Matrigel™ matrix (BD Bioscience, Franklin Lakes, NJ, USA), and the 0.1 ml aliquots were subcutaneously inoculated into the back of the BALB/c nude mice after being anesthetized with sodium pentobarbital (50 mg/kg, i.p.). When the tumor size reached an average diameter of 10–13 mm (about 2 weeks later), the *in vivo* experiments were started. The mice were randomly divided into three groups: (1) control group without treatment, (2) group with ultrasound irradiation, and (3) group with TiO_2/US treatment. Each group had six mice. After the mice were anesthetized with sodium pentobarbital (50 mg/kg, i.p.), 100 μl of the pre-S1/S2-GFP-TiO_2 NPs suspension (0.1% (w/v)) was directly injected into the tumor on the mice. The mice were then partially immersed into a water bath kept at 36 °C, and the tumor was exposed to the ultrasound using the ultrasonic apparatus (Sonic Master ES-2) under the following condition: frequency, 1 MHz; duty ratio, 50%; output power: 1 W/cm^2; and irradiation time, 60 s. The TiO_2/US treatment *in vivo* was repeated five times at days 0, 3, 6, 10 and 13, and the observation of mice was continued up to 28 days. The tumor volume was evaluated at the prescribed time points.

2.5. Evaluation for uptake of pre-S1/S2-immobilized TiO_2 NPs

The uptake of pre-S1/S2-GFP-TiO_2 NPs by HepG2 cells was evaluated by fluorescent immunocytochemistry for detecting the GFP tag on the TiO_2 NPs, according to the method described previously [27]. Anti-GFP mouse monoclonal antibody (Nakarai Tesqu, Kyoto, Japan) was used as the primary antibody, and Alexa Fluor 555 goat anti-mouse IgG antibody (Invitrogen, Carlsbad, CA, USA) and phycoerythrin-conjugated goat anti-mouse IgG antibody (Beckman Colter, Inc., Brea, CA, USA) were used as the secondary antibody for microscopy and flow cytometry, respectively. Observation of HepG2 cells was conducted using a fluorescent microscope (BZ-8000, KEYENCE, Osaka, Japan). For flow cytometry, the immunostained HepG2 cells were harvested by enzymatic treatment using a trypsin-EDTA solution (2.5 g/l trypsin (Sigma Aldrich, St. Louis, MO, USA) and 1 mM EDTA-2Na in PBS(−) buffer), and suspended in PBS(−) buffer. The fluorescent signal was detected using a flow cytometer (EPICS XL-MCL ADC, Beckman Colter, Inc., Brea, CA, USA).

2.6. Evaluation for OH radical generation

OH radical generation was evaluated by using aminophenyl fluorescein (APF, Sekisui Chemical Co., Ltd., Tokyo, Japan) which reacts with the OH radical to generate fluorescein. The TiO_2 NPs were added to the culture dishes containing 2 ml of 1 μM APF solution in PBS(−), in the absence of cells. The dish was then

irradiated with 1 MHz ultrasound at the intensities at 0–0.7 W/cm^2 for 30 s. The amount of fluorescein generated via the reaction of APF with OH radicals for 30 s was measured by a fluorescent plate reader (CytoFluor 4000, Applied Biosystems, Foster City, CA, USA) at an excitation and emission wavelength of 490 nm and 510 nm, respectively.

2.7. Evaluation for cell growth and apoptosis

Cell growth of the HepG2 were evaluated by counting the viable cells using a hemocytometer based on trypan blue exclusion, after harvesting cells by enzymatic treatment using a trypsin-EDTA solution.

Apoptosis of the HepG2 cells was evaluated based on three hallmarks, lowering of the mitochondrial membrane potential (hallmark for initiating phase of apoptosis), phosphatidylserine exposure on cell surface (for early phase of apoptosis), and nuclear chromatin condensation (for late phase of apoptosis) [33]. To detect the lowering of the mitochondrial membrane potential, HepG2 cells were stained with 5,5′,6,6′-tetrachloro-1,1′,3,3′-tetraethylbenzimidazolylcarbocyanine iodide (JC-1) using a JC-1 mitochondrial membrane potential assay kit (Cayman Chemical Company, Ann Arbor, MI, USA) per the manufacturer's instructions. In normal cells, JC-1 is incorporated into mitochondria, forming complexes with intense red fluorescence. In apoptotic cells with lower membrane potential, JC-1 remains in cytosol as the monomer, which shows green fluorescence. Red fluorescence from the JC-1 complex in mitochondria and green fluorescence from the JC-1 monomer in cytosol were observed using a fluorescent microscope (BZ-8000). To detect the phosphatidylserine externalization, HepG2 cells were stained with Annexin V using an Annexin V-FITC kit (Beckman Colter, Inc., Brea, CA, USA) because it has a high affinity for phosphatidylserine of cell membrane. Green fluorescence from fluorescein isothiocyanate (FITC) conjugated to Annexin V was observed using a fluorescent microscope. To detect the chromatin condensation, a DNA-specific fluorescent dye 4,6-diamino-2-phenylindole (DAPI) (Sigma) was used, which stains the condensed chromatin of apoptotic cells more brightly than the chromatin of normal cells. The culture dishes were washed twice with PBS(−) buffer, and the cells were immobilized with 500 μl of 4% (w/v) paraformaldehyde (PFA) solution for 30 min at room temperature (RT). After removal of the PFA solution, the cells were stained with 500 μl of 1 μg/ml DAPI solution for 30 min at RT. After washing three times with PBS(−) buffer, blue fluorescence from the DAPI-DNA complex was observed using a fluorescent microscope.

2.8. Evaluation of tumor volume

Tumor volume on the mouse xenograft model was evaluated according to the following equation. Tumor volume (mm^3) = 1/2 × (long diameter) × (short diameter)^2 [34], where long and short diameters of the tumors were measured with a slide caliper. Relative tumor volume was calculated as the ratio of the tumor volume to that before starting the TiO_2/US treatment.

2.9. Statistics

All data are presented as the means ± standard errors. Statistical analysis was performed using one-way analysis of variance (one-way ANOVA) followed by Bonferroni multiple-range test. The difference between the groups was considered to be significant when the p-value was less than 0.05.

3. Results

3.1. Uptake behavior of pre-S1/S2-immobilized TiO_2 NPs by HepG2 cells

To examine the kinetics of the pre-S1/S2 mediated uptake of TiO_2 NPs, the HepG2 cells were incubated with the pre-S1/S2-immobilized NPs for 0–24 h, and then the NPs bound to the cells was indirectly detected using GFP on the NPs as the molecular tag. Fig. 1 shows histograms of fluorescent intensity obtained from flow cytometry analysis. In the case of GFP-TiO_2 NPs (negative control), the histograms of the fluorescent signal from HepG2 cells were overlapped throughout the examined incubation time for uptake (Fig. 1A), indicating that the TiO_2 NPs without pre-S1/S2 were not incorporated by the HepG2 cells for 24 h. On the other hand, in the case of pre-S1/S2-GFP-TiO_2 NPs, the peak of the histogram was shifted to higher fluorescent intensity along with the incubation time up to 6 h, and saturated afterward (Fig. 1B). From these results, it was suggested that the incubation for 6 h was sufficient for the pre-S1/S2 mediated uptake of TiO_2 NPs by HepG2 cells.

Fig. 2 shows fluorescent images of immunostained HepG2 and WiDr cells after incubation with the TiO_2 NPs for 6 h. Uptake of the TiO_2 NPs by HepG2 cells was observed only when pre-S1/S2 was present on the NPs (Fig. 2A and B). Moreover, there was no uptake of pre-S1/S2-GFP-TiO_2 NPs by the human colon carcinoma WiDr (Fig. 2D), indicating the pre-S1/S2 mediated uptake of TiO_2

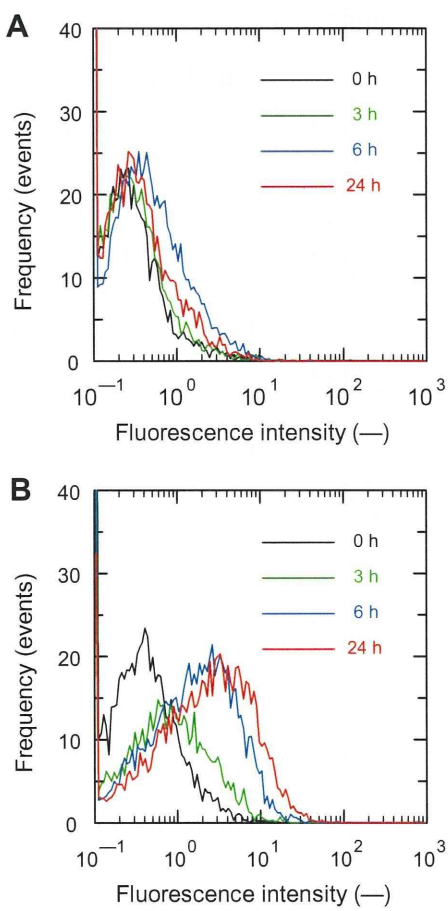

Fig. 1. Flow cytometry histograms of HepG2 cells after incubation with protein immobilized-TiO_2 NPs for 0–24 h. The uptake of GFP-TiO_2 NPs (A: negative control) and pre-S1/S2-GFP-TiO_2 NPs (B) was detected by immunostaining of HepG2 cells with anti-GFP monoclonal antibody.

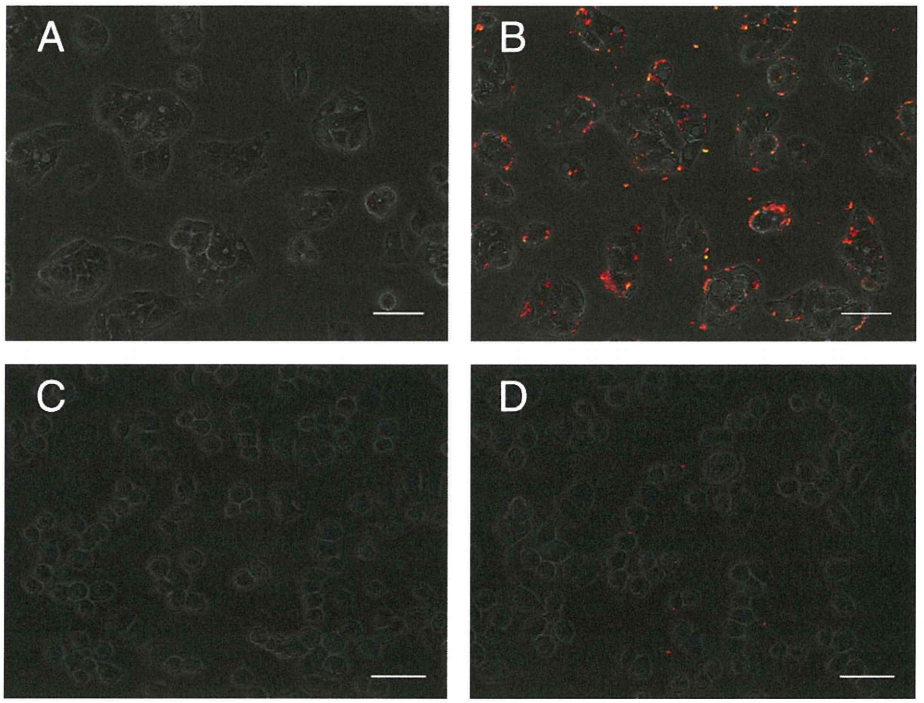

Fig. 2. Fluorescent microscopic images of HepG2 (A and B) and WiDr cells (C and D) after incubation with protein immobilized-TiO_2 NPs for 6 h. The uptake of GFP-TiO_2 NPs (A and C: negative control) and pre-S1/S2-GFP-TiO_2 NPs (B and D) was detected by immunostaining of cells with anti-GFP monoclonal antibody. Bars in the images indicate 50 μm.

NPs was specific to HepG2 cells. Therefore, these results validated the protein-immobilized TiO_2 NPs for targeted delivery toward the specific type of cells.

3.2. Effect of TiO_2/US treatment on growth and apoptosis of HepG2 cells

First, to examine the effect of ultrasound intensity on OH radical generation from TiO_2 NPs during the TiO_2/US treatment, ultrasound (0–0.7 W/cm^2) was irradiated to APF solution in the absence of cells. Fig. 3 shows the relationships between ultrasound intensity and fluorescent intensity derived from APF indicating OH radical generation. Although the OH radical was generated by the ultrasound irradiation itself, the presence of TiO_2 NPs enhanced the generation of the OH radical twice as the control, even at the lower intensity ultrasound at 0.1 W/cm^2. Therefore, ultrasound was irradiated at the intensity of 0.1 W/cm^2 in the following *in vitro* experiments.

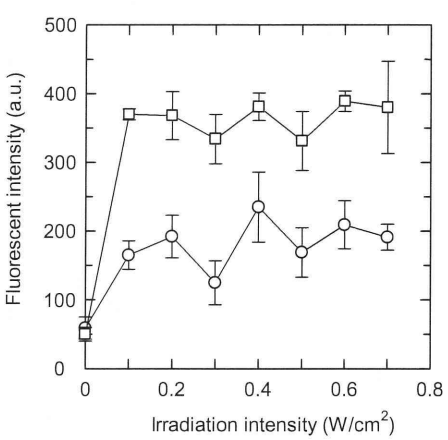

Fig. 3. Relationships between ultrasound irradiation intensity and fluorescent intensity derived from APF indicating the OH radical generated. Open circles: control with ultrasound irradiation only; open square: with addition of PAA-modified TiO_2 NPs and ultrasound irradiation. Data are the mean of three independent experiments, and the error bar indicates standard error.

Microscopic observation of HepG2 cells was conducted immediately after and at 48 h after the ultrasound irradiation to the cells with uptake of TiO_2 NPs for 6 h. Although no apparent cell damage was seen immediately after the TiO_2/US treatment (Fig. 4C), change in cellular morphology and reduction of cell number could be seen at 48 h after the TiO_2/US treatment (Fig. 4D). Therefore, to examine the effect of TiO_2/US treatment on the subsequent growth behavior of HepG2 cells, the cultures were traced for 96 h after the ultrasound irradiation to the cells with a 6 h uptake of the pre-S1/S2-GFP-TiO_2 NPs. Fig. 5 shows the time courses of viable cell numbers after the TiO_2/US treatment. In the control without treatment, the viable cell concentration increased with elapsed time, reaching 3.5×10^6 cells/ml at 96 h. In the case with ultrasound irradiation only, the growth profile was almost the same as the control condition, indicating that this low-intensity ultrasound itself had no influence on the HepG2 cell growth. Even in the case with the TiO_2/US treatment, there was no substantial decrease in viable cell numbers until 24 h compared with the other conditions. However, the cell growth rate was thereafter suppressed, and the viable cell concentration was 1.6×10^6 cells/ml at 96 h after the treatment (46% of the control). These results indicated that HepG2 cells were injured by the synergetic effect of the low-intensity ultrasound and the TiO_2 NPs incorporated to the cells. It was also indicated that the cell death was not apparent immediately after the treatment, but around 48 h after the treatment under the examined conditions.

To investigate the cell damage soon after the TiO_2/US treatment, apoptotic phenotype of the HepG2 cells was examined at 6 h after the TiO_2/US treatment. Fig. 6 shows the fluorescent images of HepG2 cells stained with JC-1, AnnexinV-FITC, and DAPI to detect

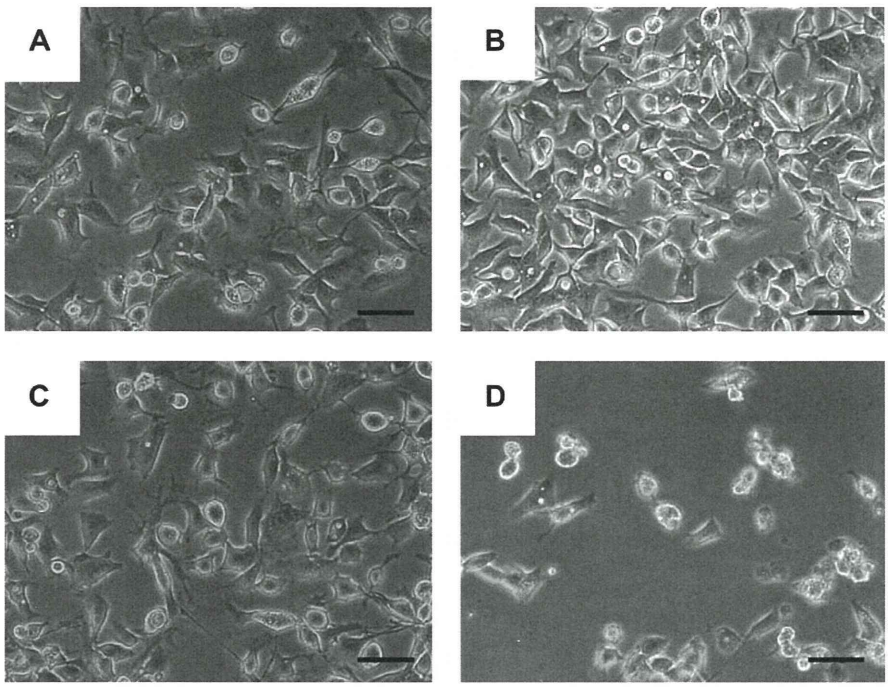

Fig. 4. Blight field microscopic images of HepG2 cells just after (A and C) and at 48 h after the treatment (B and D). (A and B) Control condition without treatment, (C and D) with TiO_2/US treatment. Each scale bar indicates 50 μm.

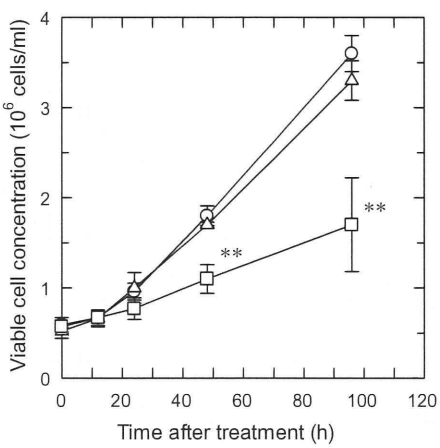

Fig. 5. Time courses of viable cell concentration of HepG2 after TiO_2/US treatment. Open circles: control condition without treatment; open triangles: with ultrasound irradiation only; open square: with TiO_2/US treatment. Data are the mean of four independent experiments, and the error bar indicates standard error. ** significantly different from the control groups ($p < 0.01$, one-way ANOVA followed by Bonferroni multiple-range test).

the lowering of the mitochondrial membrane potential (hallmark for initiating phase of apoptosis), phosphatidylserine exposure on cell surface (for early phase of apoptosis), and nuclear condensation (for late phase of apoptosis). In the case of the control without treatment, there was almost no apoptotic signal (Fig. 6A, C and E). However, in the case with the TiO_2/US treatment, the green fluorescence could be seen, indicating the loss of mitochondrial transmembrane potential (Fig. 6B) and phosphatidylserine exposure (Fig. 6D). Moreover, bright blue fluorescence derived from the condensed chromatin was also observed (Fig. 6F). From these observations, it was revealed that the TiO_2/US treatment induced the apoptosis of the HepG2 cells within 6 h after the treatment.

3.3. Anti-tumor effect of the TiO_2/US treatment

To examine the anti-tumor effect of the TiO_2/US treatment, the ultrasound was irradiated to the mouse xenograft model immediately after direct injection of pre-S1/S2-GFP-TiO_2 NPs to the tumor region. Fig. 7 shows the time courses of tumor growth on six mice in each group, where the TiO_2/US treatment was repeated five times within 13 days. In the group without treatment, the relative tumor volume in each mouse increased with elapsed time, reaching the range of 2.5–9.5 at 28 days. In the group with ultrasound irradiation only, the relative tumor volume exceeded 2.5 at 28 days in 5 mice out of 6 mice. In contrast, in the case with TiO_2/US treatment, the relative tumor volume of four mice became less than 2.5 at 28 days. These results suggested that the combination of the presence of TiO_2 NPs and ultrasound irradiation was effective in suppressing the tumor growth *in vivo*.

4. Discussion

Our previous study suggested the TiO_2/US treatment for cancer therapy, that is, SDT using the sonocatalyst TiO_2 NPs which was modified with targeting biomolecule [27]. The cell-injuring factors of the TiO_2/US treatment are considered to be roughly divided into the following: (1) Chemical factors such as the ROS generated due to the activation of TiO_2 under the ultrasound irradiation, which invites cell membrane oxidation. (2) Physical factors such as shear stress derived from the collapse of cavitation bubbles, which cause cell membrane disruption [4,26]. These chemical and physical factors observed under low-intensity ultrasound could trigger the apoptosis as well as invite the necrotic cell death mentioned above [35,36].

With regard to the chemical factor of the TiO_2/US treatment, the ROS can affect the cells more effectively when TiO_2 NPs are incorporated to the cells, since the ROS have very short half lives once they are generated on the surface of TiO_2. In this sense, it is a smart SDT strategy to modify the TiO_2 NPs with biomolecules specifically